

Indirect Probes of the MSSM after the Higgs Discovery

Wolfgang Altmannshofer,^{1,*} Marcela Carena,^{1,2,3,†} Nausheen R. Shah,^{4,‡} and Felix Yu^{1,§}

¹*Fermi National Accelerator Laboratory, P.O. Box 500, Batavia, IL 60510, USA*

²*Enrico Fermi Institute, University of Chicago, Chicago, IL 60637, USA*

³*Kavli Institute for Cosmological Physics, University of Chicago, Chicago, IL 60637, USA*

⁴*Michigan Center for Theoretical Physics, Department of Physics,
University of Michigan, Ann Arbor, MI 48109, USA*

We study the minimal supersymmetric standard model (MSSM) with minimal flavor violation (MFV), imposing constraints from flavor physics observables and MSSM Higgs searches, in light of the recent discovery of a 125 GeV Higgs boson by ATLAS and CMS. We analyze the electroweak vacuum stability conditions to further restrict the MSSM parameter space. In addition, a connection to ultraviolet physics is shown via an implementation of renormalization group running, which determines the TeV-scale spectrum from a small set of minimal supergravity parameters. Finally, we investigate the impact from dark matter direct detection searches. Our work highlights the complementarity of collider, flavor and dark matter probes in exploring the MSSM, and shows that even in a MFV framework, flavor observables constrain the MSSM parameter space well beyond the current reach of direct SUSY particle searches.

I. INTRODUCTION

Despite the null results for direct searches of supersymmetric particles at the LHC [1–29], models of supersymmetry (SUSY) remain among the most well-motivated and popular extensions of the Standard Model (SM). Besides direct searches, there exist numerous ways to indirectly probe SUSY models, *e.g.* with low energy flavor observables, from dark matter direct detection results, and through Higgs properties. The discovery of a new particle at the LHC with a mass of ~ 125 GeV compatible with a SM-like Higgs boson [30, 31] has far reaching consequences for any model of New Physics (NP) with a non-standard Higgs sector. Indeed, the LHC Higgs results have motivated numerous studies of their implications in the context of the Minimal Supersymmetric Standard Model (MSSM) and its variants [32–75].

A SM-like Higgs with a mass of $M_h \simeq 125$ GeV can be accommodated in the MSSM as long as stops are either very heavy or strongly mixed. Interestingly enough, large stop mixing unavoidably leads to irreducible contributions to low energy flavor observables, in particular in the Flavor Changing Neutral Current (FCNC) decays $B_s \rightarrow \mu^+\mu^-$ and $B \rightarrow X_s\gamma$, even if all soft masses are flavor blind. Correspondingly, rare B decays can be used to set non-trivial constraints on MSSM parameters.

In this work, we discuss the status of the MSSM, in view of the recent Higgs search results from the LHC [30, 31] and the Tevatron [76], the recent strong limits on MSSM Higgs bosons in $H/A \rightarrow b\bar{b}$ searches [78, 79] and $H/A \rightarrow \tau^+\tau^-$ searches [77], the latest results in B physics, in particular the recent evidence for $B_s \rightarrow \mu^+\mu^-$ from LHCb [80], the updated results on $B \rightarrow \tau\nu$ from

Belle [81] and BaBar [82] as well as on $B \rightarrow X_s\gamma$ from BaBar [83], and also the updated Xenon100 bounds on dark matter direct detection [84]. We will assume that the flavor structure of the SUSY particles is determined by the principle of minimal flavor violation (MFV) [85–88], *i.e.* we will assume that the SM Yukawa couplings are the only sources of flavor violation. This is motivated by the absence of any unambiguous deviation from SM expectations in flavor observables. We emphasize that even in this restrictive framework, flavor observables play an important role in constraining the viable parameter space of the MSSM. Indeed, flavor bounds can be stronger than bounds from direct searches for SUSY particles in various regions of parameter space. This is particularly true for large values of $\tan\beta$, where loop-induced flavor changing couplings of the heavy Higgs bosons of the MSSM give enhanced contributions to FCNC processes. In the MSSM with large $\tan\beta$, direct searches of the heavy Higgs bosons also become especially sensitive and, moreover, the exchange of heavy Higgs bosons can also lead to large dark matter direct detection cross sections, giving additional complementary means to probe this region of parameter space.

In the large $\tan\beta$ regime, loop corrections to Higgs-fermion couplings can be significant and it is mandatory to resum $\tan\beta$ -enhanced terms to obtain reliable predictions for any observables that depend on these couplings in the MSSM. We provide comprehensive analytical expressions for all the relevant loop-corrected Higgs couplings, loop corrections to the SM-like Higgs mass, Higgs production and decay rates, contributions to flavor observables, and dark matter direct detection cross sections, consistently taking into account the most general structure of the soft SUSY breaking terms compatible with the MFV ansatz. In particular, we include effects from the bottom Yukawa coupling as well as the tau Yukawa coupling, as they are relevant for large $\tan\beta$. This goes beyond the analyses in [89–91], where bottom Yukawa effects in the squark masses were neglected.

* waltmann@fnal.gov

† carena@fnal.gov

‡ naushah@umich.edu

§ felixyu@fnal.gov

We also give a detailed treatment of gaugino loop contributions to FCNC processes that can arise from a mass splitting between the left-handed squarks of the first two and the third generations. We highlight that in order to discuss the gaugino contributions to FCNC processes in the large $\tan\beta$ regime, both the squark mass splitting and the alignment of this splitting with the quark Yukawas must be considered.

Putting together all the relevant experimental constraints coming from current Higgs, flavor and dark matter sectors on the MSSM parameters, we point out regions of the MFV MSSM parameter space where these constraints are minimized. We also discuss the robustness of these bounds and to which extent they can be avoided. We take a phenomenological approach and treat the MSSM parameters as free parameters at the TeV scale: however, we augment this discussion with a study of renormalization group equation (RGE) effects, assuming minimal supergravity (mSUGRA)-like boundary conditions at a high scale and monitoring the generic spectrum of SUSY particles and their mass splittings induced by the running.

In Sec. II, we review the MSSM with minimal flavor violation in the quark sector. The impact of Higgs searches at the LHC and Tevatron on the MSSM are analyzed in Sec. III. We use the recent results indicating the presence of a SM-like Higgs as well as dedicated searches for the additional Higgs bosons of the MSSM. In Sec. IV, we study constraints on large $\mu \tan\beta$ from vacuum stability considerations. Constraints from B physics observables are analyzed in Sec. V. In Sec. VI, bounds on the MSSM from dark matter direct detection are considered. We conclude in Sec. VII.

II. THE MSSM WITH MINIMAL FLAVOR VIOLATION

In the following, we briefly review the MSSM with MFV. Throughout this work, in addition to MFV, we also assume minimal CP violation, *i.e.* the phase of the CKM matrix is the only source of CP violation, while all the MSSM parameters are CP conserving. We discuss the MFV structure of the sfermion masses in Sec. II A. Aspects of the Higgs spectrum that are relevant for our work are briefly reviewed in Sec. II B. In Sec. II C, we detail the $\tan\beta$ -enhanced loop corrections to the Higgs-fermion couplings, allowing for the most general squark spectrum compatible with our MFV and CP conservation assumptions.

A. Sfermion Spectrum

The soft SUSY breaking terms that give mass to the squarks, *i.e.* the soft masses, m_Q^2 , m_D^2 and m_U^2 , and trilinear couplings, A_d and A_u , are possible sources of flavor violation. Generic flavor violating entries in these matrices

are strongly constrained by flavor physics data. A simple approach to address this ‘‘SUSY flavor problem’’ is the principle of minimal flavor violation [85–88], which states that the SM Yukawa couplings are the only sources of flavor violation even in extensions of the SM. In the context of the MSSM, this implies that the soft terms can be expanded in powers of the Yukawa couplings. In the super-Cabibbo-Kobayashi-Maskawa (super-CKM) basis, where squarks and quarks are simultaneously rotated to obtain diagonal Yukawa couplings, the soft masses are [85]

$$\begin{aligned}\hat{m}_Q^2 &= \tilde{m}_Q^2 (1 + b_1 V^\dagger y_u^2 V + b_2 y_d^2 \\ &\quad + b_3 (y_d^2 V^\dagger y_u^2 V + V^\dagger y_u^2 V y_d^2)) , \\ \hat{m}_U^2 &= \tilde{m}_U^2 (1 + b_4 y_u^2) , \\ \hat{m}_D^2 &= \tilde{m}_D^2 (1 + b_5 y_d^2) ,\end{aligned}\tag{1}$$

where y_u and y_d are the diagonal up and down quark Yukawa matrices and V is the CKM matrix. The soft mass \hat{m}_Q^2 enters the left-left block of the down squark mass matrix, while $V\hat{m}_Q^2 V^\dagger$ enters the up squark mass matrix. The generic structure in (1) is always generated by RGE running if flavor blind boundary conditions are assumed at a high scale [92, 93]. The parameters b_i lead to splittings between the squark masses. To be specific, the parameters b_4 and b_5 generate a splitting between the masses of the first two and the third generations of right-handed up and down squarks, respectively, while the parameters b_1 , b_2 , and b_3 generate a splitting between the first two and the third generations of left-handed squarks. Note that the parameters b_2 , b_3 , and b_5 only become important for large values of $\tan\beta$, where the bottom Yukawa is $\mathcal{O}(1)$. As we are particularly interested in the large $\tan\beta$ regime, in the following we will take all the above masses as independent parameters and use $m_{Q_3}^2$, $m_{D_3}^2$, and $m_{U_3}^2$ for the stop and sbottom masses and m_Q^2 , m_D^2 , and m_U^2 for the masses of the first two generations, which are degenerate to an excellent approximation in this setup. This is analogous to the pMSSM framework [94] frequently studied in the literature.

We stress, however, that the parameters b_1 , b_2 , and b_3 also induce flavor violating entries in the left-handed squark mass matrices. These entries are proportional to small CKM angles and lead to controlled but non-negligible contributions to FCNC processes. In fact, due to $SU(2)_L$ invariance, the left-left blocks of the up and down squark mass matrices are related by a CKM rotation, and therefore *any splitting* in the diagonal entries of the left-handed soft masses \hat{m}_Q^2 unavoidably induces off-diagonal entries in the up or down squark mass matrices. Moreover, distinct flavor phenomenology arises depending on which of the b_1 , b_2 , or b_3 parameters is responsible for the splitting. In particular, a splitting induced by b_1 (b_2) is aligned in the up- (down-) sector and will only lead to off-diagonal entries in the down (up) squark mass matrix. The parameter b_3 induces flavor violation in both the up and down squark masses matrices. All flavor observables that we will discuss in the following

depend on the combination $b_1 + b_3 y_b^2$. We thus introduce one additional parameter

$$\zeta = \frac{b_1 y_t^2 + b_3 y_b^2 y_t^2}{b_1 y_t^2 + b_2 y_b^2 + 2b_3 y_b^2 y_t^2}, \quad (2)$$

which reflects the alignment of the splitting in the left-handed squark masses and hence parametrizes the fraction of the splitting in the masses leading to flavor violation in the down sector. We assume ζ is real in the following.¹ We see that formally $\zeta = 1 + \mathcal{O}(y_b^2)$. If we consider a splitting in the squark masses that is radiatively induced through RGE running, then considering only the top Yukawa in the running leads to $\zeta = 1$. Bottom Yukawa effects become important for large $\tan\beta$ and can lead to $0 < \zeta < 1$. Typically we expect that y_b is at most as large as y_t , however, which implies $1/2 < \zeta < 1$.

We note that an expansion analogous to (1) also exists for the trilinear couplings [85]. In particular, higher order terms in the expansion can lead to flavor violating trilinear terms. Such terms only lead to corrections of the holomorphic Higgs couplings, however. These corrections can induce flavor changing neutral Higgs couplings, that are especially interesting beyond MFV, where the corresponding effects can be chirally enhanced [95, 96]. In the MFV framework considered here, these effects are less important compared to contributions that are related to the loop-induced non-holomorphic Higgs couplings. The only relevant trilinear couplings for our analysis are those for the third generation squarks, A_t and A_b , which we will take to be independent parameters.

For simplicity, we will also assume universal soft masses m_L^2 and m_E^2 , in the slepton sector. The phenomenology of flavor non-universalities in the lepton sector will be reserved for future study. The only relevant trilinear term in the slepton sector is the tau trilinear coupling A_τ , which, along with A_t and A_b and all other parameters, we will take to be real.

B. Higgs Spectrum

The physical Higgs spectrum of the MSSM consists of two neutral scalar bosons h and H , one neutral pseudoscalar A , and a pair of charged Higgs bosons H^\pm . At tree level, the full spectrum is determined by only two real parameters: the mass of the pseudoscalar Higgs, M_A , and the ratio of the two vacuum expectation values, $\tan\beta = t_\beta = v_u/v_d$, with $v_u^2 + v_d^2 = v^2 = 174^2 \text{ GeV}^2$. In the so-called decoupling limit, $M_A^2 \gg M_W^2$, the masses of the Higgs bosons, A , H and H^\pm , are

$$M_H^2 \simeq M_A^2, \quad M_{H^\pm}^2 \simeq M_A^2 + M_W^2. \quad (3)$$

¹ Note that while b_1 and b_2 have to be real due to hermiticity of the squark masses, b_3 can in principle be complex. Indeed, as shown in [93], a tiny phase for b_3 is always generated during RGE running.

In this limit, the mass of the lightest Higgs h is given at tree level by

$$M_h^2 \simeq M_Z^2 \cos 2\beta. \quad (4)$$

As is well known, moderate or large values of $\tan\beta$ and large 1-loop corrections are required to lift M_h up to phenomenologically viable values. Moreover, at large $\tan\beta$, the sbottom and stau 1-loop corrections can lower M_h by a few GeV, which cannot be neglected given the current Higgs mass precision data. The dominant stop, sbottom, and stau loop contributions for large $\tan\beta$ read

$$\begin{aligned} \Delta M_h^2 \simeq & \frac{3}{4\pi^2} \frac{m_t^4}{v^2} \left[\log\left(\frac{m_{\tilde{t}}^2}{m_t^2}\right) + \frac{X_t^2}{m_{\tilde{t}}^2} - \frac{X_t^4}{12m_{\tilde{t}}^4} \right] \\ & - \frac{3}{48\pi^2} \frac{m_b^4}{v^2} \frac{t_\beta^4}{(1 + \epsilon_b t_\beta)^4} \frac{\mu^4}{m_{\tilde{b}}^4} \\ & - \frac{1}{48\pi^2} \frac{m_\tau^4}{v^2} \frac{t_\beta^4}{(1 + \epsilon_\tau t_\beta)^4} \frac{\mu^4}{m_{\tilde{\tau}}^4}, \end{aligned} \quad (5)$$

where $X_t = A_t - \mu/\tan\beta \approx A_t$ for large $\tan\beta$, and $m_{\tilde{t}}$, $m_{\tilde{b}}$ and $m_{\tilde{\tau}}$ are the average stop, sbottom, and stau masses, respectively. The stop loop corrections, reported in the first line of (5), are maximized for $A_t \simeq \sqrt{6}m_{\tilde{t}}$. The contributions from the sbottom and stau loops, in the second and third lines, always reduce the light Higgs mass and can be particularly important for large $\tan\beta$, large values of the Higgsino mass parameter, μ , and light sbottom or stau masses [97]. The ϵ_i factors come from an all-order resummation of $\tan\beta$ enhanced corrections to the Higgs-fermion couplings and are discussed in detail in Sec. II C.

The couplings of the lightest Higgs to SM fermions and gauge bosons are mainly controlled by $\tan\beta$ and the angle α that diagonalizes the mass matrix of the two scalar Higgs bosons. If

$$\alpha = \beta - \pi/2, \quad (6)$$

the couplings of h are exactly SM-like. At the tree level, Eq. (6) holds up to corrections of order $M_Z^2/(t_\beta M_A^2)$. Correspondingly, for large $\tan\beta$ and moderately heavy M_A , the couplings of h are already SM-like to a good approximation. At 1-loop, Eq. (6) gets corrected by an additional term $\sim \lambda_7 v^2/M_A^2$, where λ_7 is a loop-induced quartic Higgs coupling that reads

$$\begin{aligned} \lambda_7 \simeq & \frac{3}{96\pi^2} \frac{m_t^4}{v^4} \frac{\mu A_t}{m_{\tilde{t}}^2} \left(\frac{A_t^2}{m_{\tilde{t}}^2} - 6 \right) \\ & + \frac{3}{96\pi^2} \frac{m_b^4}{v^4} \frac{t_\beta^4}{(1 + \epsilon_b t_\beta)^4} \frac{\mu^3 A_b}{m_{\tilde{b}}^4} \\ & + \frac{1}{96\pi^2} \frac{m_\tau^4}{v^4} \frac{t_\beta^4}{(1 + \epsilon_\tau t_\beta)^4} \frac{\mu^3 A_\tau}{m_{\tilde{\tau}}^4}. \end{aligned} \quad (7)$$

If λ_7 is sizable, corrections to the light Higgs couplings can become relevant, as discussed in the next section, and are constrained by the SM Higgs searches at the LHC.

C. Higgs Couplings to Fermions

At tree level, the MSSM Higgs sector is a 2 Higgs doublet model of type II, where only H_u couples to right-handed up quarks and only H_d couples to right-handed down quarks and leptons. The Yukawa interactions thus have the following form

$$\begin{aligned} \mathcal{L}_{\text{Yuk}} = & (y_u)_{ij} H_u \bar{Q}_i U_j + (y_d)_{ij} H_d \bar{Q}_i D_j \\ & + (y_\ell)_{ij} H_d \bar{L}_i E_j + \text{h.c.} \end{aligned} \quad (8)$$

As a consequence, the couplings of the neutral Higgs bosons to fermions are flavor diagonal in the mass eigenstate basis. At the loop level, however, “wrong” Higgs couplings are generated and lead to potentially large threshold corrections to the masses of down type quarks and leptons [98–101] as well as CKM matrix elements [102]. They also significantly modify charged Higgs couplings to quarks [103, 104] and generate flavor changing neutral Higgs couplings [95, 96, 105–110]. All these effects become particularly relevant in the large $\tan\beta$ regime, where the inherent 1-loop suppression can be partly compensated. In the following, we analyze the form of the neutral and charged Higgs couplings with fermions in the phenomenologically motivated limit, $v^2 \ll M_{\text{SUSY}}^2$ (see [110] for a discussion of the regime $v^2 \sim M_{\text{SUSY}}^2$). We consistently take into account the most generic MFV structure of the squark masses as discussed in Sec. II A. In particular, we consider splittings between the first two and the third generation squarks in the left-handed as well as right-handed sectors.

Once the 1-loop corrections are taken into account and we have diagonalized the quark mass matrices, the couplings of the neutral Higgs mass eigenstates to fermions have the following generic form

$$\begin{aligned} \mathcal{L}_{\text{int}} \supset & \sum_{q,q'} \frac{m_q}{\sqrt{2}v} (\bar{q}'_L q_R) (\xi_{q'q}^h h + \xi_{q'q}^H H + i\xi_{q'q}^A A) \\ & + \sum_{\ell} \frac{m_\ell}{\sqrt{2}v} (\bar{\ell}_L \ell_R) (\xi_\ell^h h + \xi_\ell^H H + i\xi_\ell^A A) + \text{h.c.} \end{aligned} \quad (9)$$

where we have neglected flavor changing couplings to leptons, which are not relevant for our analysis. Using the notation $\xi_{qq}^i = \xi_q^i$, and again for large $\tan\beta$, the flavor conserving couplings of the heavy scalar and pseudoscalar Higgses, normalized to their respective SM Yukawas, are

$$-\xi_q^H \simeq \xi_q^A \simeq \frac{1}{t_\beta} - \epsilon_q, \quad \text{for } q = u, c, t, \quad (10)$$

$$\xi_q^H \simeq \xi_q^A \simeq \frac{t_\beta}{1 + \epsilon_q t_\beta}, \quad \text{for } q = d, s, b, \quad (11)$$

$$\xi_\ell^H \simeq \xi_\ell^A \simeq \frac{t_\beta}{1 + \epsilon_\ell t_\beta}. \quad (12)$$

In the above expressions, $\tan\beta$ -enhanced corrections to the couplings are resummed to all orders and the ϵ_i factors parametrize the loop induced “wrong” Higgs couplings. The exact form of each ϵ_i in terms of MSSM parameters is discussed at the end of this section. Since

we assume the MSSM parameters to be CP conserving, all ϵ_i parameters are real.

Among the flavor changing Higgs couplings only the coupling of a right handed bottom with a left-handed strange quark will be relevant in the following discussion. Normalized to the bottom Yukawa of the SM, we have

$$\xi_{sb}^H \simeq \xi_{sb}^A \simeq \frac{\epsilon_{\text{FC}} t_\beta^2}{(1 + \epsilon_b t_\beta)(1 + \epsilon_0 t_\beta)} V_{tb} V_{ts}^*, \quad (13)$$

where ϵ_0 is defined as $\epsilon_0 = \epsilon_b - \epsilon_{\text{FC}}$, and ϵ_{FC} is discussed in detail below.

The couplings of the light Higgs boson, h , are exactly SM-like in the decoupling limit: $\xi_q^h = \xi_\ell^h = 1$ and $\xi_{q'q}^h = 0$ for $q' \neq q$. While non-standard effects in the couplings to up-type quarks are generically tiny even away from the decoupling limit, corrections to the couplings with down-type quarks and leptons decouple very slowly and can be relevant. We have

$$\xi_f^h = -\frac{s_\alpha}{c_\beta} \frac{1 - \epsilon_f/t_\alpha}{1 + \epsilon_f t_\beta}, \quad \text{for } f = d, s, b, \ell. \quad (14)$$

The couplings of the physical charged Higgs bosons to fermions can be written as

$$\begin{aligned} \mathcal{L}_{\text{int}} \supset & \sum_{q,q'} \frac{m_q}{v} (\bar{q}'_L q_R) \xi_{q'q}^\pm H^\pm \\ & + \sum_{\ell} \frac{m_\ell}{v} (\bar{\nu}'_L \ell_R) \xi_{\nu\ell}^\pm H^\pm + \text{h.c.} \end{aligned} \quad (15)$$

For the couplings relevant to our analysis, we have

$$\frac{\xi_{tb}^\pm}{V_{tb}} = \frac{t_\beta}{1 + \epsilon_b t_\beta}, \quad \frac{\xi_{us}^\pm}{V_{us}} = \frac{t_\beta}{1 + \epsilon_s t_\beta}, \quad (16)$$

$$\frac{\xi_{ub}^\pm}{V_{ub}} = \frac{\xi_{cb}^\pm}{V_{cb}} = \frac{t_\beta}{1 + \epsilon_0 t_\beta}, \quad \xi_{\nu\ell}^\pm = \frac{t_\beta}{1 + \epsilon_\ell t_\beta}, \quad (17)$$

$$\frac{\xi_{st}^\pm}{V_{ts}^*} = \frac{1}{t_\beta} - \epsilon'_0 + \epsilon'_{\text{FC}} \frac{\epsilon_{\text{FC}} t_\beta}{1 + \epsilon_0 t_\beta}, \quad (18)$$

where V_{ij} are CKM matrix elements and $\epsilon'_0 = \epsilon_t - \epsilon'_{\text{FC}}$. The parameter ϵ'_{FC} is the up-sector analogue of ϵ_{FC} .

As already mentioned, the various ϵ factors in the above expressions parametrize loop-induced non-holomorphic Higgs couplings. They arise from Higgsino-squark loops, gluino-squark loops and wino-sfermion loops. We do not explicitly state the typically negligible contributions coming from bino-sfermion loops; however, they are included in our numerical analysis.

For the bottom quark, we can decompose $\epsilon_b = \epsilon_b^{\tilde{g}} + \epsilon_b^{\tilde{W}} + \epsilon_b^{\tilde{H}}$, where these contributions are

$$\epsilon_b^{\tilde{g}} = \frac{\alpha_s}{4\pi} \frac{8}{3} \mu M_3 g(M_3^2, m_{Q_3}^2, m_{D_3}^2), \quad (19)$$

$$\epsilon_b^{\tilde{W}} = -\frac{\alpha_2}{4\pi} \frac{3}{2} \mu M_2 g(\mu^2, M_2^2, m_{Q_3}^2), \quad (20)$$

$$\epsilon_b^{\tilde{H}} = \frac{\alpha_2}{4\pi} \frac{m_t^2}{2M_W^2} \mu A_t g(\mu^2, m_{Q_3}^2, m_{U_3}^2). \quad (21)$$

The loop function g is listed in the appendix, and has units of $(\text{GeV})^{-2}$. Hence, the ϵ factors generally exhibit non-decoupling as the SUSY mass scale increases. In particular, rescaling all the SUSY mass parameters, *i.e.* the squark masses, gaugino masses, the Higgsino mass parameter and the trilinear coupling by a common, arbitrarily large factor, leaves the ϵ parameters invariant. For a degenerate SUSY spectrum with mass \tilde{m} , we obtain $g(\tilde{m}^2, \tilde{m}^2, \tilde{m}^2) = 1/2\tilde{m}^2$. Our sign convention is that the left-right mixing entries in the top and bottom squark mass matrices are given by $m_t(A_t - \mu \cot \beta)$ and $m_b(A_b - \mu \tan \beta)$, respectively. Furthermore, the gluino mass M_3 is always positive in our convention.

For the strange and down quarks, the Higgsino contribution is highly suppressed by small Yukawa couplings or CKM angles and only the gluino and wino loops are relevant: $\epsilon_{s,d} = \epsilon_{s,d}^{\tilde{g}} + \epsilon_{s,d}^{\tilde{W}}$, where the $\epsilon_{s,d}^i$ can be easily obtained from the corresponding ϵ_b^i expressions, replacing third generation squark masses with second or first generation squark masses.

For leptons, only the wino (and the bino) loops give contributions, and $\epsilon_\ell^{\tilde{W}}$ is given by $\epsilon_b^{\tilde{W}}$ with the sbottom masses replaced by the slepton masses.

In case of the top quark, analogous to the bottom quark, we consider the gluino, wino, and Higgsino contributions: $\epsilon_t = \epsilon_t^{\tilde{g}} + \epsilon_t^{\tilde{W}} + \epsilon_t^{\tilde{H}}$. The expressions for $\epsilon_t^{\tilde{g}}$ and $\epsilon_t^{\tilde{W}}$ are trivially obtained from the corresponding ϵ_b^i by replacing the relevant squark masses. The Higgsino contribution is explicitly given by

$$\epsilon_t^{\tilde{H}} = -\frac{\alpha_2}{4\pi} \frac{m_b^2}{2M_{\tilde{W}}^2} \frac{t_\beta^2}{(1 + \epsilon_b t_\beta)^2} \mu A_b g(\mu^2, m_{Q_3}^2, m_{D_3}^2). \quad (22)$$

Here, $\epsilon_t^{\tilde{H}}$ is suppressed by the bottom quark mass and only becomes relevant for large values of $\tan \beta$.

The flavor changing couplings, ϵ_{FC} and ϵ'_{FC} , can be decomposed as

$$\epsilon_{\text{FC}} = \epsilon_b^{\tilde{H}} + \zeta \epsilon_{\text{FC}}^{\tilde{g}} + \zeta \epsilon_{\text{FC}}^{\tilde{W}}, \quad (23)$$

$$\epsilon'_{\text{FC}} = \epsilon_t^{\tilde{H}} + (1 - \zeta) \epsilon_{\text{FC}}^{\prime \tilde{g}} + (1 - \zeta) \epsilon_{\text{FC}}^{\tilde{W}}, \quad (24)$$

with

$$\epsilon_{\text{FC}}^{\tilde{g}} = \frac{\alpha_s}{4\pi} \frac{8}{3} \mu M_{\tilde{g}} \times (g(M_3^2, m_{Q_3}^2, m_{D_3}^2) - g(M_3^2, m_Q^2, m_{D_3}^2)), \quad (25)$$

$$\epsilon_{\text{FC}}^{\tilde{W}} = -\frac{\alpha_2}{4\pi} \frac{3}{2} \mu M_2 \times (g(\mu^2, M_2^2, m_{Q_3}^2) - g(\mu^2, M_2^2, m_Q^2)), \quad (26)$$

and $\epsilon_{\text{FC}}^{\prime \tilde{g}}$ is obtained from $\epsilon_{\text{FC}}^{\tilde{g}}$ by replacing the right-handed sbottom mass, m_{D_3} , with the right-handed stop mass, m_{U_3} . The $\epsilon_b^{\tilde{H}}$ and $\epsilon_t^{\tilde{H}}$ expressions were already given above. Note that m_{D_3} enters both loop functions in (25) and hence, in general, $\epsilon_{\text{FC}}^{\tilde{g}} \neq \epsilon_b^{\tilde{g}} - \epsilon_s^{\tilde{g}}$, in contrast to the case where all right-handed down squarks have the same mass, $m_{D_3} = m_D$. Clearly, a splitting between the

third and the first two generations of left-handed squarks induces non-zero $\epsilon_{\text{FC}}^{\tilde{g}}$, $\epsilon_{\text{FC}}^{\tilde{W}}$ and/or $\epsilon_{\text{FC}}^{\prime \tilde{g}}$.

As already described in Sec. II A, ζ parametrizes the alignment of the left-handed squark mass with the quark masses. The case $\zeta = 1$ corresponds to a m_Q^2 that is aligned in the up sector such that the mass splitting between the first two and the third generations leads to off-diagonal entries only in the down squark mass matrix. This in turn implies maximal flavor changing gaugino loop corrections to the Higgs–down quark couplings. The case $\zeta = 0$ corresponds to alignment in the down sector, with no off-diagonal entries appearing in the down squark mass matrix. Generically, from RGE running, we expect $1/2 < \zeta < 1$.

III. HIGGS COLLIDER SEARCHES

A. SM-like 125 GeV Higgs

The LHC experiments, ATLAS and CMS, have recently discovered a new particle with a mass of about 125 GeV [30, 31]. This discovery is based on results from SM Higgs searches in the $\gamma\gamma$, ZZ and WW channels. The observed signals indicate that the new particle is a boson with spin 0 or 2, and overall, they are in reasonable agreement with expectations for a SM Higgs. Other searches in the $\tau^+\tau^-$ and bb decay channels are also being pursued, but more statistics are needed in order to make conclusive statements.

The most visible feature of the extracted signal strength in all the different channels under study is an enhancement in the $\gamma\gamma$ decay rate in comparison to the SM rate. The decay rates into WW and ZZ gauge bosons are consistent with the SM values at the 1σ level. The present experimental uncertainties in the signal strength in the various production and decay channels allow for many new physics alternatives. In particular, within supersymmetric extensions, it is possible to enhance or suppress the gluon fusion production with light stops, depending on the amount of mixing in the stop sector. It is also possible to suppress gluon fusion with light sbottoms that have sizable mixing driven by large values of $\mu \tan \beta$. In all cases, enhancement of gluon fusion implies a suppression of the $h \rightarrow \gamma\gamma$ decay rate, and vice-versa. The overall effective $gg \rightarrow h \rightarrow \gamma\gamma$ rate, however, is governed by the enhancement or suppression of the gluon fusion production cross section.

To achieve a net enhancement in the $h \rightarrow \gamma\gamma$ rate, uncorrelated with a simultaneous enhancement in the $h \rightarrow WW/ZZ$ rates coming from an enhanced gluon fusion production or reduced $h \rightarrow b\bar{b}$ partial width, the existence of new, light, charged colorless particles running in the loop is required. In the MSSM, the only two options are charginos, which only contribute for $\tan \beta \sim 1$ (disfavored by a 125 GeV Higgs mass), and light staus with large mixing, *i.e.* large $\mu \tan \beta$. A detailed discussion of the possible deviations from SM values of the produc-

tion and decay rates for a SM-like Higgs in the MSSM can be found in [39, 58]. Possible correlations with flavor observables have very recently been studied in [75].

While it is very interesting to investigate deviations from SM expectations in Higgs data that would point towards new SUSY particles within the reach of the LHC, we take a different approach in this work by assuming a Higgs boson with approximately SM-like properties. We concentrate on possible signatures of new physics that may appear in B physics observables, direct non-SM Higgs searches and dark matter direct detection searches within the MSSM with MFV, while fulfilling the requirement of a 125 GeV SM-like Higgs. In this way, we show indirect effects from SUSY particles in flavor and Higgs physics in regions of parameter space beyond the present reach of the LHC.

B. Searches for Heavy Scalars and Pseudoscalars

Searches for the heavy neutral Higgs bosons of the MSSM have been performed in the $H/A \rightarrow bb$ and $H/A \rightarrow \tau^+\tau^-$ channels both at the Tevatron [111–114] and the LHC [77–79, 115, 116].

Searches also exist for light charged Higgs bosons in top decays at both the Tevatron [117, 118] and the LHC [119–121]. For the MSSM scenarios considered in this work, however, the corresponding bounds are not competitive with the bounds from searches of the neutral Higgs bosons.

In the large $\tan\beta$ regime, the cross sections for the heavy scalar and pseudoscalar Higgses rescale according to

$$\sigma_{bb \rightarrow H} \simeq \sigma_{bb \rightarrow A} \simeq \sigma_{bb \rightarrow h}^{\text{SM}} \times \frac{t_\beta^2}{(1 + \epsilon_b t_\beta)^2}, \quad (27)$$

$$\begin{aligned} \sigma_{gg \rightarrow H} \simeq \sigma_{gg \rightarrow A} \simeq \sigma_{gg \rightarrow h}^{tt, \text{SM}} \times \left(\frac{1}{t_\beta} - \epsilon_t \right)^2 \\ + \sigma_{gg \rightarrow h}^{tb, \text{SM}} \times \frac{1 - \epsilon_t t_\beta}{1 + \epsilon_b t_\beta} + \sigma_{gg \rightarrow h}^{bb, \text{SM}} \times \frac{t_\beta^2}{(1 + \epsilon_b t_\beta)^2}, \end{aligned} \quad (28)$$

evaluated at a common mass for all Higgs bosons. For large $\tan\beta$, the $\sigma_{bb \rightarrow H/A}$ production cross sections can dominate over gluon fusion. We use HIGLU [122] and `bbh@nnlo` [123] to compute the respective SM cross sections $\sigma_{gg \rightarrow h}^{i, \text{SM}}$ and $\sigma_{bb \rightarrow h}^{\text{SM}}$ at the LHC.

The most important decay modes of the heavy Higgs bosons are $H, A \rightarrow bb$ and $H, A \rightarrow \tau^+\tau^-$. The corresponding partial widths can be written as

$$\Gamma_{Hbb} \simeq \Gamma_{Abb} \simeq \Gamma_{hbb}^{\text{SM}} \times \frac{t_\beta^2}{(1 + \epsilon_b t_\beta)^2}, \quad (29)$$

$$\Gamma_{H\tau\tau} \simeq \Gamma_{A\tau\tau} \simeq \Gamma_{h\tau\tau}^{\text{SM}} \times \frac{t_\beta^2}{(1 + \epsilon_\tau t_\beta)^2}, \quad (30)$$

where Γ_{hff}^{SM} are the corresponding decay widths of a Higgs boson with the same mass as H and A and with SM-like

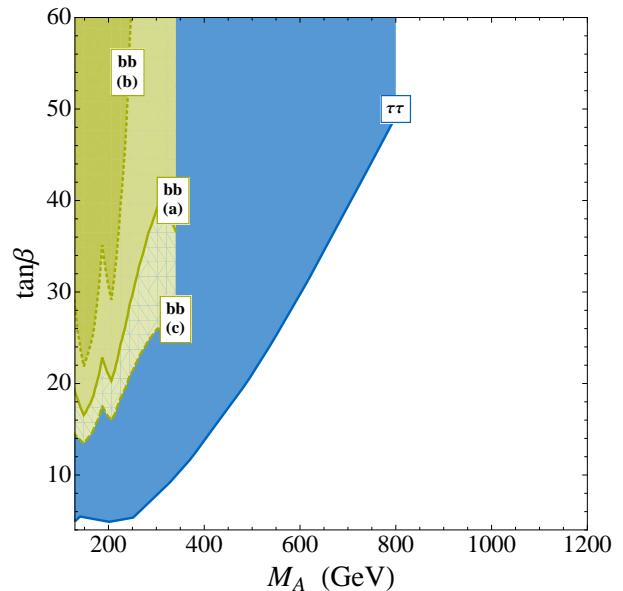


FIG. 1. Constraints in the M_A – $\tan\beta$ plane from direct searches of the neutral MSSM Higgs bosons at CMS and ATLAS. The solid, dotted and dashed lines correspond to scenarios (a), (b), and (c) as defined in Tab. I. The blue (green) regions are excluded by searches in the $\tau^+\tau^-$ (bb) channel.

Scenario	(a)	(b)	(c)	(d)	(e)
μ [TeV]	1	4	-1.5	1	-1.5
$\text{sign}(A_t)$	+	+	+	-	-

TABLE I. Illustrative MSSM scenarios discussed in the text. All sfermion masses are set to a common value 2 TeV, the gaugino masses to $6M_1 = 3M_2 = M_3 = 1.5$ TeV. The trilinear couplings $A_t = A_b = A_\tau$ are set such that the lightest Higgs mass is $M_h = 125$ GeV.

couplings to bb and $\tau^+\tau^-$. In our numerical analysis, we compute Γ_{hff}^{SM} using HDECAY [124].

Note that the main dependence of the production cross sections and branching ratios is on $\tan\beta$ and the heavy Higgs masses. Dependence on other MSSM parameters enters only at the loop level through the $\tan\beta$ resummation factors ϵ_i .

In our framework, the most important constraints come from the CMS bounds in the $\tau^+\tau^-$ channel [77], which are available up to masses of $M_A = 800$ GeV and the $b\bar{b}$ channel [78, 79] which cover heavy Higgs masses up to $M_A < 350$ GeV. Our estimates for the excluded regions from the $H/A \rightarrow b\bar{b}$ searches are shown in Fig. 1 in yellow-green and labeled with bb . We set all sfermion masses to 2 TeV and the gaugino masses to $6M_1 = 3M_2 = M_3 = 1.5$ TeV. The solid, dotted and dashed contours correspond to a Higgsino mass parameter $\mu = 1$ TeV (scenario a), 4 TeV (scenario b) and -1.5

TeV (scenario c), respectively. For every point in the M_A - $\tan\beta$ plane, the trilinear couplings $A_t = A_b = A_\tau$ are positive and chosen such that the lightest Higgs mass, computed using `FeynHiggs` [125], is $M_h = 125$ GeV.² The respective choices for μ lead to representative values for the $\tan\beta$ resummation factors of $\epsilon_b^{\tilde{g}} + \epsilon_b^{\tilde{W}} \simeq 3.3 \times 10^{-3}$, 1.5×10^{-2} and -5.1×10^{-3} .

As is well known, the bounds in the M_A - $\tan\beta$ plane coming from the $\tau^+\tau^-$ channel are robust against variations of the MSSM parameters. Indeed, the dependence of the production cross section on ϵ_b is largely cancelled by the corresponding dependence of the $\text{BR}(A, H \rightarrow \tau^+\tau^-)$ [126, 127]. In Fig. 1, we therefore simply report in blue the $\tan\beta$ bounds obtained in [77] in the so-called M_h^{max} scenario. We checked explicitly that the constraints are largely independent of the scenarios in Tab. I. We find that the constraints can only be weakened mildly for large $\tan\beta$ and M_A if the MSSM parameters are such that ϵ_b is sizable and positive, as in scenario (b)³. We note however, that in the region with low $\tan\beta$, the bounds do depend to some extent on the SUSY spectrum, in particular the neutralino and chargino spectrum. Indeed, for low $\tan\beta$, the heavy scalar and pseudoscalar Higgs bosons can have sizable branching ratios in neutralinos or charginos if these decays are kinematically allowed. The M_h^{max} scenario considered in [77] contains light neutralinos with $M_{\chi_1} \simeq 95$ GeV. For small $\tan\beta$, the obtained bounds from the searches in the $\tau^+\tau^-$ channel are therefore slightly weaker compared to scenarios with heavier neutralinos.

The CMS searches in the bb channel [78, 79] are not yet competitive with the $\tau^+\tau^-$ searches, but might become important for large M_A in the future [128]. Compared to the $\tau^+\tau^-$ searches, the bounds coming from the bb searches show a stronger dependence on the remaining MSSM parameters [126, 127]. In particular, for large negative μ , the bounds become significantly stronger, while for large positive μ , the bounds can be weakened considerably. Note that for large negative μ and large $\tan\beta$, however, constraints from vacuum stability and perturbativity of the bottom Yukawa have to be taken into account.

Since the theoretical precision of the light Higgs mass prediction in the MSSM allows shifts of a few GeV, we checked the extent to which the $H/A \rightarrow \tau^+\tau^-$ and $H/A \rightarrow b\bar{b}$ bounds depend on the exact value of the Higgs

mass assumed in our analysis, $M_h = 125$ GeV. We find that varying the light Higgs mass in the range 122 GeV $< M_h < 128$ GeV does not change the constraints from H and A searches significantly.

IV. VACUUM STABILITY

Independent of experimental searches, large values of μ can be constrained based on vacuum stability considerations, particularly if $\tan\beta$ is also large. Indeed, large values of $\mu \tan\beta$ can lead to charge and color breaking minima in the scalar potential of the MSSM [129].

The trilinear couplings of the up-type Higgs, H_u , with sbottoms, \tilde{b}_L and \tilde{b}_R , and staus, $\tilde{\tau}_L$ and $\tilde{\tau}_R$, are controlled by

$$\mathcal{L} \supset \frac{m_\tau}{v} \frac{\mu \tan\beta}{1 + \epsilon_\tau \tan\beta} (H_u^0 \tilde{\tau}_L^* \tilde{\tau}_R) + \frac{m_b}{v} \frac{\mu \tan\beta}{1 + \epsilon_b \tan\beta} (H_u^0 \tilde{b}_L^* \tilde{b}_R) + \text{h.c.} \quad (31)$$

For trilinear couplings that are large compared to the sbottom or stau masses, minima with non-zero vevs for the sbottom and/or stau fields can arise in addition to the standard electroweak minimum. If these minima are deeper than the electroweak minimum, the electroweak minimum becomes unstable and can decay. The corresponding regions of parameter space are only viable as long as the lifetime of the electroweak minimum is longer than the age of the universe. This corresponds to requiring that the bounce action, B , of the tunneling process is $B \gtrsim 400$ [130, 131].

Our phenomenological flavor analysis is largely independent of the values of the stau masses, and non-zero stau vevs can always be avoided if $m_{\tilde{\tau}_L}$ and $m_{\tilde{\tau}_R}$ are large enough. Nonetheless, we will consider a scenario where the squark and slepton masses are the same order and thus include both sbottoms and staus in the following analysis.

Starting with the MSSM scalar potential, we restrict ourselves to terms that contain only the up-type Higgs, sbottoms, and staus, which are the degrees of freedom most relevant for large $\mu \tan\beta$. We consider three cases: (i) only terms with the up-type Higgs and staus, (ii) only up-type Higgs and sbottoms, and (iii) up-type Higgs, staus and sbottoms simultaneously. In each case, we search for additional minima in field space and estimate the bounce action for tunneling from the electroweak minimum into the deepest minimum of the potential. In the end, we apply the strongest of the three bounds.

For each case, the second vacuum generally has separately nearly degenerate stau vevs and nearly equal sbottom vevs. In the case of the sbottoms, this is expected from the $SU(3)$ D -terms in the scalar potential:

$$\mathcal{L} \supset \frac{g_s^2}{6} \left(|\tilde{b}_L|^2 - |\tilde{b}_R|^2 \right)^2 \quad (32)$$

² The Higgs mass, M_h , is not a monotonic function in A_t and for a given sign of A_t there are typically two choices of A_t that lead to $M_h = 125$ GeV. We always take the A_t that is smaller in magnitude.

³ The CMS results in the $\tau^+\tau^-$ channel are only available as constraints in the M_A - $\tan\beta$ plane for the M_h^{max} scenario. We translate these constraints into bounds on the corresponding $\sigma \times \text{BR}$ and then reinterpret the cross section bounds as constraints in the M_A - $\tan\beta$ plane for various choices of the other MSSM parameters summarized in Tab. I. We assume constant efficiencies throughout this procedure.

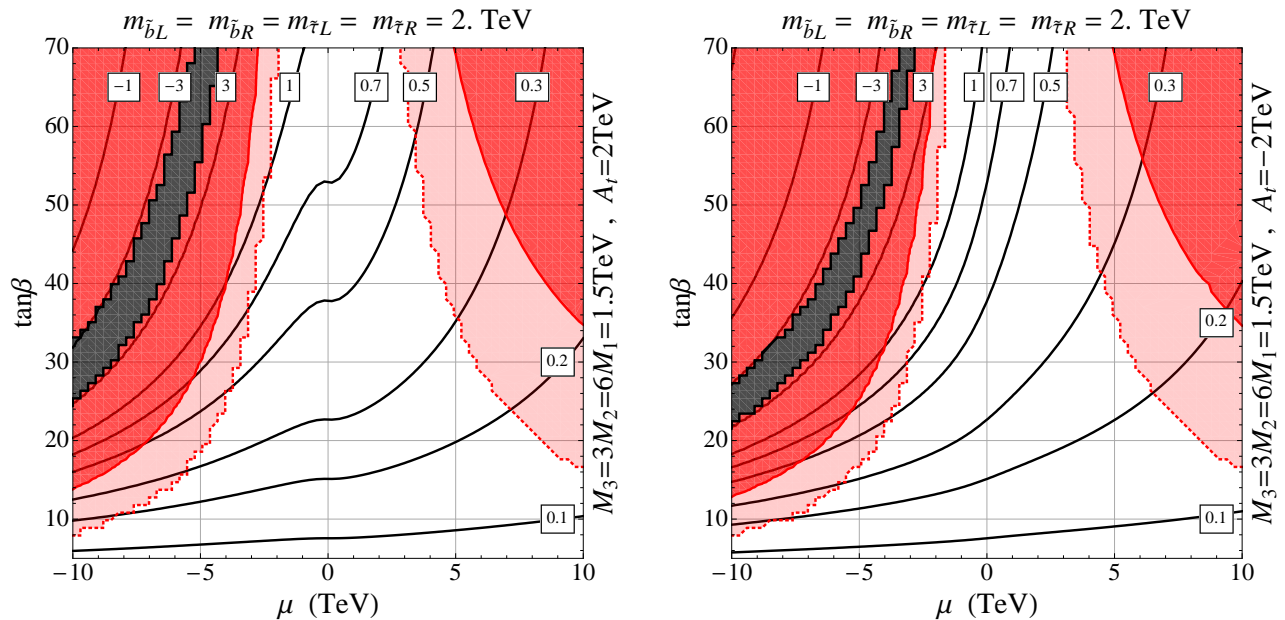


FIG. 2. Constraints from vacuum stability in the μ - $\tan\beta$ plane. We set the sbottom and stau soft masses to 2 TeV and the gaugino masses to $6M_1 = 3M_2 = M_3 = 1.5$ TeV. In the left (right) plot, the trilinear coupling of the stops is $A_t = 2$ TeV ($A_t = -2$ TeV). The labeled contours show the values of the bottom Yukawa coupling. In the light red (light gray) regions, a charge and color breaking vacuum exists that is deeper than the electroweak breaking vacuum, but the electroweak vacuum has a lifetime that is longer than the age of the universe. In the dark red (gray) regions, the electroweak vacuum is not stable on cosmological time scales. Finally, in the black regions, one of the sbottoms becomes tachyonic.

We can clearly see that at least for the 3-dimensional parameter space in case (ii), deviations from equality of the squark/slepton fields along the path chosen to compute the action would come at the expense of large contributions from the D terms. Therefore, to obtain an analytical estimate for the bounce action, we consider a straight path in field space connecting the electroweak minimum and the charge and/or color breaking minimum.

We then approximate the potential along the straight line by a triangle and use the analytical expressions in [132] to calculate the bounce action. We construct the triangle such that for a few chosen parameter points, the obtained bounce action agrees approximately with the bounce action from the analytic expression of the potential solved numerically by a standard overshoot/undershoot method. We further crosschecked our results with *CosmoTransitions* [133] taking into account the up-type Higgs, the down-type Higgs, the sbottoms, and the staus. Overall, we find good agreement with our approximate analytical approach.

The constraints thus derived in the μ - $\tan\beta$ plane are shown in Fig. 2. We fix the SUSY masses as in the scenarios considered above, namely we assume degenerate sfermion masses with $\tilde{m} = 2$ TeV and gaugino masses with $6M_1 = 3M_2 = M_3 = 1.5$ TeV. The trilinear couplings we set to $A_t = 2$ TeV in the left and to $A_t = -2$ TeV in the right plot. In the white region, the electroweak minimum is the deepest minimum in the potential and therefore absolutely stable. In the light red (light gray) region, a charge (and possibly color) break-

ing minimum exists that is deeper than the electroweak minimum, but the electroweak minimum has a lifetime longer than the age of the universe. In the dark red (gray) region the lifetime of the electroweak minimum is shorter than the age of the universe. Finally, in the black region, one of the sbottoms is tachyonic.

The solid lines labeled in the plots show contours of constant bottom Yukawa couplings in the μ - $\tan\beta$ plane. For large and negative $\mu \tan\beta$, close to the region where one of the sbottoms becomes tachyonic, the bottom Yukawa coupling becomes non perturbatively large.

We observe that large negative values for μ are strongly constrained by the requirement of vacuum stability. This is because the $\tan\beta$ resummation factor, ϵ_b , in (31) is linearly proportional to μ . It increases the trilinear coupling of the up-type Higgs with sbottoms for negative values of μ and can lead to a deep second minimum mainly in the field direction of the sbottoms. In particular, we find that values of $\mu \tan\beta$ negative and large enough that the bottom Yukawa changes its sign (the parameter space in the upper left corner of the plot beyond the region excluded by tachyonic sbottoms) are excluded by the requirement of vacuum stability. For positive values of μ , the coupling of the up-type Higgs with sbottoms is reduced while its coupling with staus is slightly enhanced by the ϵ_τ term. In this region of parameter space, constraints come typically from a second minimum in the stau direction. Positive values for μ are less constrained than negative ones, and the allowed region for μ can be extended above $\mu > 10$ TeV for sufficiently heavy staus.

The viable regions of parameter space can be enlarged slightly when we allow for a splitting between the masses of the left- and right-handed sbottoms and staus. Nevertheless, we do not find any regions of parameter space where both vacuum stability and $\epsilon_b \tan \beta < -1$ (which flips the sign of the tree level bottom Yukawa and hence changes the typical sign of the SUSY contribution to B observables) can be achieved simultaneously. In the end, we see that the scenarios discussed in the previous section are all compatible with bounds from vacuum stability.

V. B PHYSICS OBSERVABLES

Flavor observables play a crucial role in determining viable regions of parameter space of SUSY models. This is true both under the MFV assumption [89–91, 134–140] and if new sources of flavor violation are allowed [141–150].

Of particular importance in the MFV setup are rare B decays that are helicity suppressed in the SM, because SUSY contributions to these decays can be enhanced by $\tan \beta$ factors. Interesting processes include the tree level decay $B \rightarrow \tau\nu$, the purely leptonic decay $B_s \rightarrow \mu^+\mu^-$, and the radiative decay $B \rightarrow X_s\gamma$. Additional constraints on the SUSY parameter space can be also derived from the $(g-2)$ of the muon. The $(g-2)_\mu$ bound becomes particularly important if sleptons are only moderately heavy, which is a scenario that we do not consider here.

A. $B \rightarrow \tau\nu$, $B \rightarrow D^{(*)}\tau\nu$ and $K \rightarrow \mu\nu$

The decay $B \rightarrow \tau\nu$ is a sensitive probe of extended Higgs sectors as it can be modified by charged Higgs exchanges at tree level [151]. The most important inputs for the SM prediction are the CKM element $|V_{ub}|$ and the B meson decay constant. Using the PDG value $|V_{ub}| = (3.89 \pm 0.44) \times 10^{-3}$ [152], a conservative average over direct determinations from inclusive and exclusive semi-leptonic B decays, and an average of recent precise lattice determinations of the decay constant $f_B = (190 \pm 4) \text{ MeV}$ [153–156], we find

$$\text{BR}(B \rightarrow \tau\nu)_{\text{SM}} = (0.97 \pm 0.22) \times 10^{-4}. \quad (33)$$

While previous experimental data gave values for the branching ratio more than 2σ above the SM prediction, a recent result from Belle [81] has a much lower central value. An average of all the available data from BaBar [82, 157] and Belle [81, 158] gives

$$\text{BR}(B \rightarrow \tau\nu)_{\text{exp}} = (1.16 \pm 0.22) \times 10^{-4}. \quad (34)$$

This value is in very good agreement with the SM but still leaves room for NP contributions.

Closely related decay modes that are also sensitive to charged Higgs effects are the $B \rightarrow D\tau\nu$ and $B \rightarrow D^*\tau\nu$

decays [159–163]. While predictions of the corresponding branching ratios suffer from large hadronic uncertainties coming from the $B \rightarrow D$ and $B \rightarrow D^*$ form factors, the ratios $\text{BR}(B \rightarrow D\tau\nu)/\text{BR}(B \rightarrow D\ell\nu)$ and $\text{BR}(B \rightarrow D^*\tau\nu)/\text{BR}(B \rightarrow D^*\ell\nu)$, where $\ell = e$ or μ , can be predicted with reasonable accuracy in the SM [162, 164]. Interestingly, recent results from BaBar [165] on these ratios are around 2σ above the SM predictions in both decay modes. Older results from Belle [166] give similar central values but with much larger uncertainties.

Another interesting observable in this context is $R_{\mu 23}$ [167] that probes the tree level charged Higgs exchange in the $K \rightarrow \mu\nu$ decay. The much smaller sensitivity of $K \rightarrow \mu\nu$ to charged Higgs effects compared to the B decays is compensated by its extremely high experimental precision and the excellent control on theoretical uncertainties giving [167]

$$R_{\mu 23} = 0.999 \pm 0.007. \quad (35)$$

All the mentioned tree level decays depend in similar ways on possible new physics contributions in the MSSM with MFV. Defining

$$X_{B(K)}^2 = \frac{1}{M_{H^\pm}^2} \frac{t_\beta^2}{(1 + \epsilon_{0(s)} t_\beta)(1 + \epsilon_\ell t_\beta)}, \quad (36)$$

we can write

$$R_{B\tau\nu} = \frac{\text{BR}(B \rightarrow \tau\nu)}{\text{BR}(B \rightarrow \tau\nu)_{\text{SM}}} = \left(1 - m_{B^+}^2 X_B^2\right)^2, \quad (37)$$

$$R_{D\tau\nu} = \frac{\text{BR}(B \rightarrow D\tau\nu)}{\text{BR}(B \rightarrow D\tau\nu)_{\text{SM}}} = \left(1 - 1.5 m_\tau m_b X_B^2 + 1.0 m_\tau^2 m_b^2 X_B^4\right), \quad (38)$$

$$R_{D^*\tau\nu} = \frac{\text{BR}(B \rightarrow D^*\tau\nu)}{\text{BR}(B \rightarrow D^*\tau\nu)_{\text{SM}}} = \left(1 - 0.12 m_\tau m_b X_B^2 + 0.05 m_\tau^2 m_b^2 X_B^4\right), \quad (39)$$

$$R_{\mu 23} = \frac{\text{BR}(K \rightarrow \mu\nu)}{\text{BR}(K \rightarrow \mu\nu)_{\text{SM}}} = \left(1 - m_{K^+}^2 X_K^2\right). \quad (40)$$

In Fig. 3 we show these ratios as function of $X_{B,K} = \sqrt{|X_{B,K}^2|}$ both for positive X_i^2 (solid lines) and negative X_i^2 (dotted lines) in comparison with the experimental 1σ and 2σ ranges (dashed bands) from (33)-(35) and [162]-[165]. Here, positive X_i^2 illustrates destructive interference with the SM, while negative X_i^2 illustrates constructive interference with the SM.

We observe that agreement of theory and experiment in all three B observables is impossible to achieve. In particular the tensions in $B \rightarrow D\tau\nu$ and $B \rightarrow D^*\tau\nu$ cannot be addressed in the context of the MSSM with MFV, but require more radical approaches [168–172].

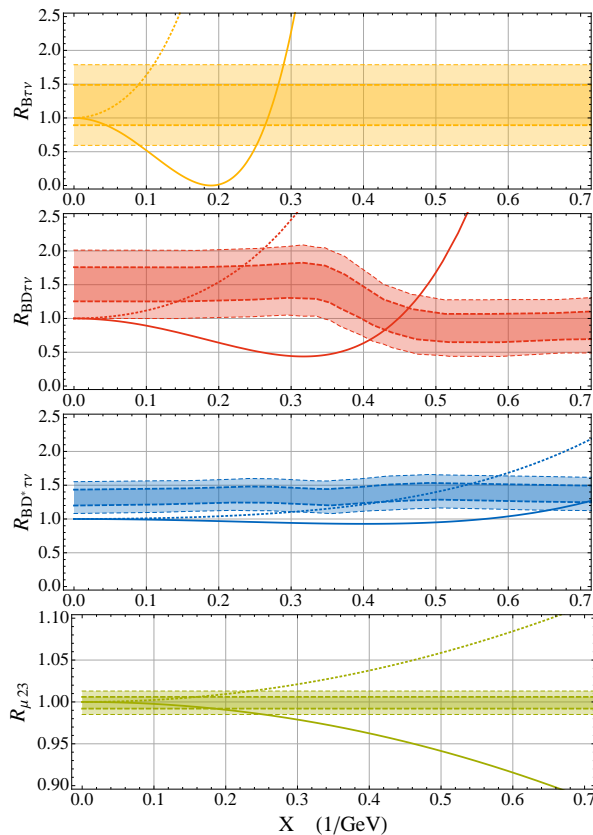


FIG. 3. Branching ratios of the decays $B \rightarrow \tau\nu$, $B \rightarrow D\tau\nu$, $B \rightarrow D^*\tau\nu$, and $K \rightarrow \mu\nu$ as functions of X_B , $X_K = \sqrt{|X_{B,K}^2|}$ as appropriate and which are defined in the main text. The dashed bands show the 1σ and 2σ experimental ranges. The solid (dotted) lines are the theory predictions for positive (negative) X^2 giving destructive (constructive) interference with the SM amplitude.

Considering MSSM contributions to $K \rightarrow \mu\nu$ and $B \rightarrow \tau\nu$, we observe that generally, X_B and X_K are equal to a good approximation. The only way to induce a difference is through a splitting between the right-handed strange squark mass and the right-handed bottom squark mass which enter the corresponding ϵ factors in the definitions of X_B and X_K . As discussed in Sec. II A, such a splitting is compatible with the MFV ansatz for the squark spectrum as long as $\tan\beta$ is large enough that y_b effects cannot be neglected. However, we find that even for a large mass splitting $X_B \simeq X_K$ holds, except for regions of parameter space with large and negative μ , such that $\epsilon_{0(s)} \tan\beta \sim \mathcal{O}(-1)$. Such regions of parameter space are strongly constrained by perturbativity of the bottom Yukawa and vacuum stability considerations, as discussed in Sec. IV. If $X_B \simeq X_K$, then the $B \rightarrow \tau\nu$ decay gives stronger constraints than $K \rightarrow \mu\nu$.⁴

⁴ For the special range $0.25 \lesssim X_B, X_K \lesssim 0.30$ and $\epsilon_0 \tan\beta >$

In the following, we therefore concentrate on the constraint from $B \rightarrow \tau\nu$ on the MSSM parameter space. Apart from corners of parameter space with very large and negative $\epsilon_0 \tan\beta < -1$, the charged Higgs contribution interferes destructively with the SM ($X_B^2 > 0$), and leads to constraints in the $M_{H^\pm} - \tan\beta$ plane. These constraints depend on other SUSY parameters only through the loop-induced $\tan\beta$ resummation factors ϵ_i and are therefore robust in large parts of parameter space.

The yellow lines in the left plot of Fig. 4 show the $B \rightarrow \tau\nu$ constraints in the $M_A - \tan\beta$ plane corresponding to the 3 choices of MSSM parameters (a), (b), and (c) given in Tab. I and already discussed in Sec. III B. For comparison, the constraint from direct searches in the $\tau^+\tau^-$ channel is also shown in gray. There are also a narrow strips of small Higgs masses and large $\tan\beta$ where the NP contribution to the $B \rightarrow \tau\nu$ amplitude is twice as large as the SM contribution. This in turn implies that this region of parameters is in principle allowed by the experimental data on $B \rightarrow \tau\nu$. It is in strong tension, however, with the results from $B \rightarrow D\tau\nu$, $B \rightarrow D^*\tau\nu$, and $K \rightarrow \mu\nu$ and furthermore is excluded by direct searches.

The dependence of the $B \rightarrow \tau\nu$ constraints on the $\tan\beta$ resummation factors is stronger than the one of the direct searches in the $\tau^+\tau^-$ channel, especially for large values of $\tan\beta$. For large values of $\tan\beta$ and a positive (negative) value of ϵ_0 the constraint can be weakened (strengthened) considerably. As ϵ_0 does not depend on A_t , the constraint from $B \rightarrow \tau\nu$ is to a large extent insensitive to the exact value of the light Higgs mass. Constraints from direct MSSM Higgs searches are generically stronger for $M_A < 800$ GeV. While the latest results from direct MSSM Higgs searches in the $\tau^+\tau^-$ channel at the LHC end at $M_A = 800$ GeV, obviously no such restriction exists for the $B \rightarrow \tau\nu$ constraints. Only very large values of $\tan\beta \gtrsim 60$, however, are typically probed by $B \rightarrow \tau\nu$ for such large heavy Higgs masses.

In corners of parameter space with very large negative μ , we can have $\epsilon_0 \tan\beta < -1$ for values of $\tan\beta$ that are not extremely large and when the bottom Yukawa is perturbative [140]. Such a situation is shown in the right plot of Fig. 4, where $\mu = -8$ TeV and the resulting $\epsilon_0 \simeq -0.03$. For $\tan\beta \lesssim 30$, the charged Higgs still interferes destructively with the SM. For larger values of $\tan\beta \gtrsim 30$, however, the sign of X_B^2 flips, the interference becomes constructive, and the branching ratio is always enhanced. This behavior can be seen from the values of $R_{B\tau\nu}$ indicated with the dotted contours in the right plot of Fig. 4.

Note that vacuum stability requirements, however, strongly constrain very large and negative values of μ . As discussed in Sec. IV, we do not find viable regions of parameter space where the bottom Yukawa has a negative

—1, the $K \rightarrow \mu\nu$ constraint is stronger than $B \rightarrow \tau\nu$, but this parameter region is excluded by direct searches as discussed in the main text.

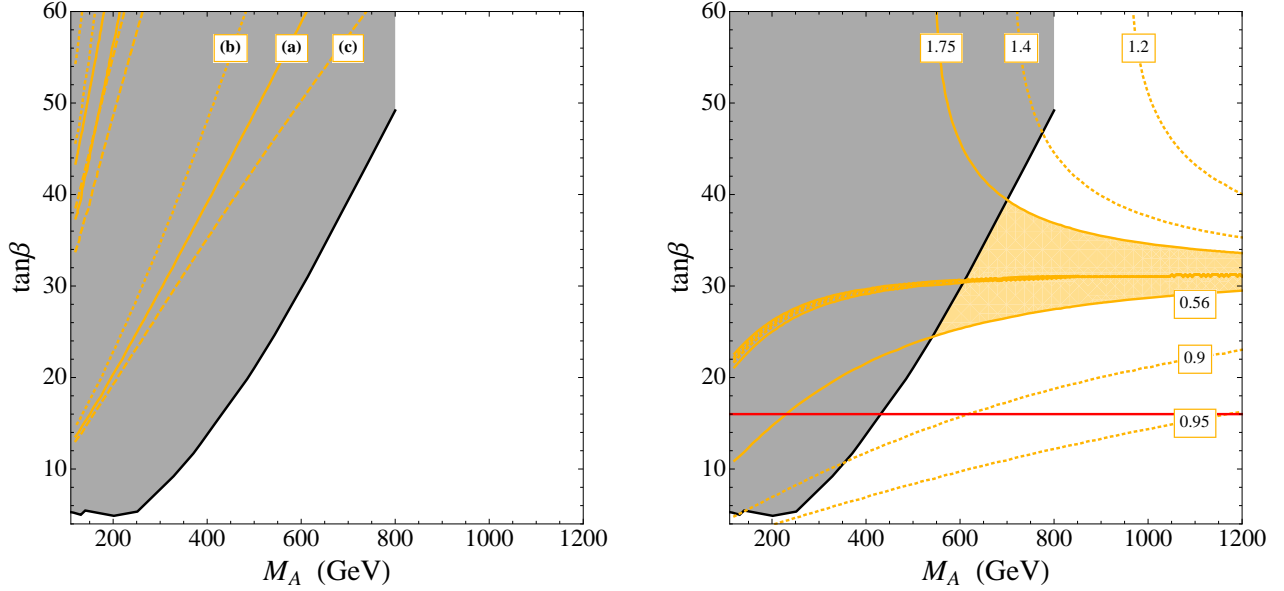


FIG. 4. Constraints in the M_A - $\tan\beta$ plane from the tree level $B \rightarrow \tau\nu$ decay. The constraint from direct heavy Higgs searches is also shown in gray. The yellow solid, dotted and dashed contours in the left plot correspond to scenarios (a), (b), and (c) defined in Tab. I. The right plot shows a scenario with $\mu = -8$ TeV, leading to a large negative ϵ_0 such that the charged Higgs contribution interferes constructively with the SM in the region with $\tan\beta \gtrsim 30$. The labeled contours indicate values for $R_{B\tau\nu}$. Above the red horizontal line, the electroweak vacuum has a lifetime shorter than the age of the universe.

sign with respect to the SM one, *i.e.* with $\epsilon_b \tan\beta < -1$. For $B \rightarrow \tau\nu$, the relevant parameter combination is $\epsilon_0 \tan\beta$. The horizontal red line in the right plot of Fig. 4 marks the upper bound on $\tan\beta$ in the scenario with $\mu = -8$ TeV, such that the electroweak vacuum remains stable on timescales of the age of the universe. Therefore, we see that $\epsilon_0 \tan\beta < -1$ is also excluded by vacuum stability considerations. This conclusion holds beyond the discussed $\mu = -8$ TeV example.

B. $B_s \rightarrow \mu^+\mu^-$

The $B_s \rightarrow \mu^+\mu^-$ decay is a flavor changing neutral current process and correspondingly only induced at the loop level, both in the SM and the MSSM. In the SM, $B_s \rightarrow \mu^+\mu^-$ is also helicity suppressed by the muon mass, resulting in a tiny SM prediction, at the level of 10^{-9} . Using the recently given precise value for the B_s meson decay constant $f_{B_s} = (227 \pm 4)$ MeV [156] which is an average of several lattice determinations [153–155], and taking into account the effect of the large width difference in the B_s meson system [173, 174], we have the branching ratio extracted from an untagged rate as [175] (see also [176])

$$\text{BR}(B_s \rightarrow \mu^+\mu^-)_{\text{SM}} = (3.32 \pm 0.17) \times 10^{-9}. \quad (41)$$

Experimental searches for that decay have been carried out at D0 [177] and CDF [178], and are ongoing at ATLAS [179], CMS [180], and LHCb [80, 181]. Very recently,

the LHCb collaboration reported first evidence for the $B_s \rightarrow \mu^+\mu^-$ decay [80]. LHCb finds for the branching ratio the following value

$$\text{BR}(B_s \rightarrow \mu^+\mu^-)_{\text{exp}} = (3.2^{+1.4}_{-1.2} {}^{+0.5}_{-0.3}) \times 10^{-9}, \quad (42)$$

and gives the following two sided 95% C.L. bound

$$1.1 \times 10^{-9} < \text{BR}(B_s \rightarrow \mu^+\mu^-)_{\text{exp}} < 6.4 \times 10^{-9}. \quad (43)$$

We use this bound in our analysis. Note that the upper bound in (43) is considerably *weaker* than the official combination of the previous LHCb result [181] with the ATLAS and CMS bounds [182].

For large values of $\tan\beta$, order of magnitude enhancements of the $\text{BR}(B_s \rightarrow \mu^+\mu^-)$ are possible in the MSSM [106, 183]. In the large $\tan\beta$ limit, the CP averaged branching ratio in the MFV MSSM can be written to a good approximation as

$$R_{B_s\mu\mu} = \frac{\text{BR}(B_s \rightarrow \mu^+\mu^-)}{\text{BR}(B_s \rightarrow \mu^+\mu^-)_{\text{SM}}} \simeq |\mathcal{A}|^2 + |1 - \mathcal{A}|^2. \quad (44)$$

The MSSM contribution \mathcal{A} is dominated by so-called Higgs penguins, *i.e.* the exchange of the heavy scalar H and pseudoscalar A with their 1-loop induced flavor changing $b \rightarrow s$ couplings, that are parametrized by ϵ_{FC} given in (13). We find

$$\mathcal{A} = \frac{4\pi}{\alpha_2} \frac{m_{B_s}^2}{4M_A^2} \frac{\epsilon_{\text{FC}} t_\beta^3}{(1 + \epsilon_b t_\beta)(1 + \epsilon_0 t_\beta)(1 + \epsilon_t t_\beta)} \frac{1}{Y_0}. \quad (45)$$

The SM loop function Y_0 depends on the top mass and is approximately $Y_0 \simeq 0.96$. Note that the MSSM contributions to $B_s \rightarrow \mu^+\mu^-$ do not decouple with the scale of the SUSY particles, but with the masses of the heavy scalar and pseudoscalar Higgs bosons $M_H^2 \simeq M_A^2$. Due to the strong enhancement by $\tan^3 \beta$, the large $\tan \beta$ regime of the MSSM is highly constrained by the current experimental results on $\text{BR}(B_s \rightarrow \mu^+\mu^-)$. We remark, however, that ϵ_{FC} in the numerator of (45) is a sum of several terms (see (23)) each of which depend strongly on several MSSM parameters. In addition, cancellations among the different terms can occur in certain regions of parameter space, rendering the $B_s \rightarrow \mu^+\mu^-$ constraint very model dependent, even in the restrictive framework of MFV. Additional contributions to $B_s \rightarrow \mu^+\mu^-$ can arise from charged Higgs loops [187]. They interfere destructively with the SM contribution and scale as $(\tan \beta)^2/M_{H^\pm}^2$. Typically, their effect is considerably smaller compared to the SUSY contribution in (45).

We stress that there is a simple mathematical lower bound of $R_{B_s\mu\mu} = 1/2$ in (44) that is saturated for $\mathcal{A} = 1/2$. In this case, the SUSY contribution partially cancels the SM amplitude, but simultaneously generates a non-interfering piece that cannot be canceled. This lower limit provides a significant threshold for experiments searching for $\text{BR}(B_s \rightarrow \mu^+\mu^-)$: not only is the SM branching fraction a meaningful value to test experimentally, but the potential observation of the branching fraction below one half of the SM value would strongly indicate NP and imply departure from the MSSM with MFV. Note that the current 2σ lower bound from LHCb on the branching ratio is below 1/2 of the SM value and therefore does not lead to constraints in our framework, yet.

In Fig. 5, we show the constraints from $B_s \rightarrow \mu^+\mu^-$ in the M_A - $\tan \beta$ plane. The red solid, dotted and dashed contours correspond to scenarios (a), (b), and (c) of Tab. I. The dash-dotted contour corresponds to scenario (d), with all MSSM parameters as for the solid contour, but with a negative sign for the trilinear coupling. For comparison, the constraints from direct searches are again shown in gray. As expected, we observe a very strong dependence of the $B_s \rightarrow \mu^+\mu^-$ bounds on the choices of the remaining MSSM parameters, particularly the sign of μA_t . Note that in the considered scenarios, we assume degenerate squarks such that the only term entering ϵ_{FC} is from the irreducible Higgsino loop contribution, $\epsilon_b^{\tilde{H}}$, whose sign is dictated by μA_t . For positive (negative) μA_t the NP contribution interferes destructively (constructively) with the SM amplitude. Since the lower bound on $\text{BR}(B_s \rightarrow \mu^+\mu^-)$ from LHCb is still below half of the SM value, destructively interfering NP is much less constrained than constructively interfering NP.

The plots of Fig. 6 show in red the constraints from $B_s \rightarrow \mu^+\mu^-$ in the plane of the third generation squark masses and the Higgsino mass parameter μ . The gray horizontal band corresponds to the constraint from direct searches of charginos at LEP that exclude $|\mu| \lesssim$

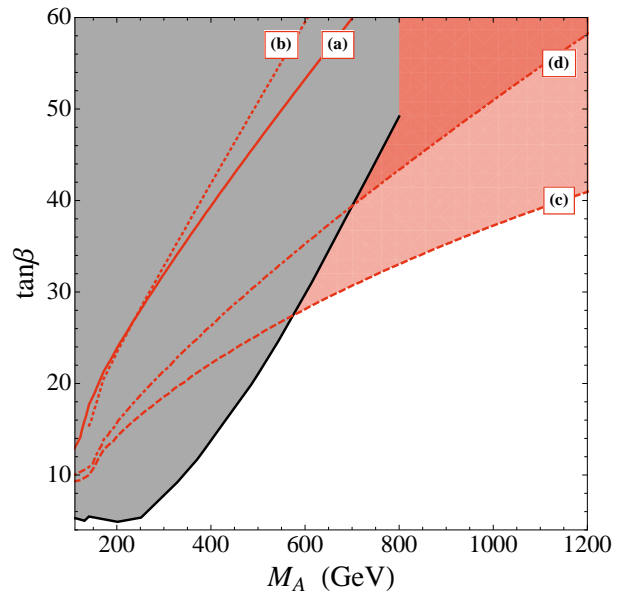


FIG. 5. Constraints in the M_A - $\tan \beta$ plane from the $B_s \rightarrow \mu^+\mu^-$ decay. The red solid, dotted, dashed and dash-dotted contours correspond to scenarios (a), (b), (c) and (d), as described in the text. The gray region is excluded by direct searches of MSSM Higgs bosons in the $H/A \rightarrow \tau^+\tau^-$ channel.

100 GeV [184, 185]. In these plots, we fix $M_A = 800$ GeV, $\tan \beta = 45$ (fully compatible with the $B \rightarrow \tau\nu$ constraint and not yet constrained by direct searches), and gaugino masses with $6M_1 = 3M_2 = M_3 = 1.5$ TeV. As in all the other plots, we vary the trilinear couplings $A_t = A_b = A_\tau$ throughout the plot such that the lightest Higgs mass is $M_h = 125$ GeV. The values for A_t are indicated in the plots by the vertical dotted contours. The two plots correspond to positive and negative values of the A -terms. In the gray region in the lower left corners of the plots, the sbottom loop corrections to the lightest Higgs mass become so large that the lightest Higgs mass is always below $M_h < 125$ GeV for any value of A_t , taking into account a 3 GeV theory uncertainty. We checked that varying the light Higgs mass between $122 \text{ GeV} < M_h < 128 \text{ GeV}$ can change the values of A_t by around 25% in each direction and therefore can affect the constraints derived from $B_s \rightarrow \mu^+\mu^-$ at a quantitative level. However, the qualitative picture of the constraints and the interplay of the SUSY contributions to $B_s \rightarrow \mu^+\mu^-$, as discussed below, are unaffected by this variation.

The solid contours are obtained under the assumption that the masses of the first two generation squarks are equal to the third generation, while for the dashed and dotted contours we assume the first two generations to be heavier by 50%. For the dashed contours, we assume the splitting for the left-handed squarks to be fully aligned in the up-sector, such that gaugino-squark loops also contribute to ϵ_{FC} with $\zeta = 1$ (see (23) and (25)). We set $\zeta = 0.5$ for the dotted contours, such that only

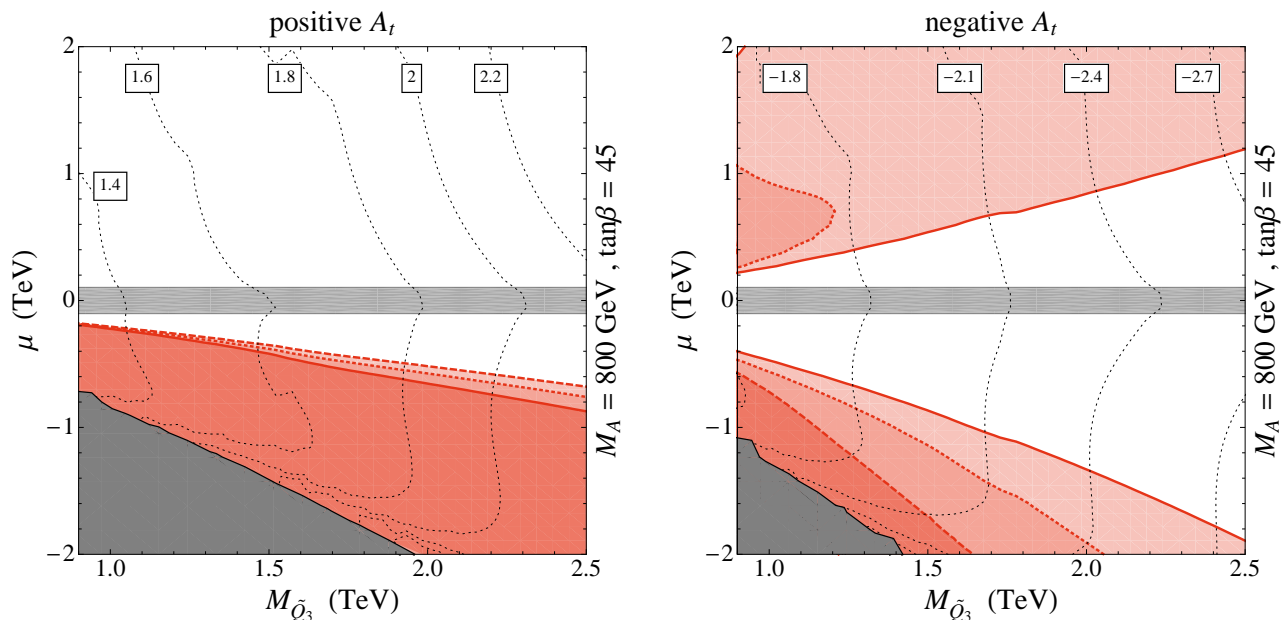


FIG. 6. Constraints in the $m_{Q_3}-\mu$ plane from the $B_s \rightarrow \mu^+\mu^-$ decay, with fixed $M_3 = 3M_2 = 6M_1 = 1.5$ TeV, $M_A = 800$ GeV and $\tan\beta = 45$. The solid bounded regions correspond to a degenerate squark spectrum. The dashed and dotted boundaries correspond to choosing the first two squark generations 50% heavier than the third generation squark masses, with an alignment of $\zeta = 1$ and $\zeta = 0.5$, respectively. The gray horizontal band corresponds to the constraint from direct searches of charginos at LEP. The vertical dotted lines show contours of constant A_t such that $M_h = 125$ GeV. In the gray regions in the lower left corners, the lightest Higgs mass is always below $M_h < 125$ GeV, taking into account a 3 GeV theory uncertainty.

half of the squark mass splitting induces flavor violation in the down-sector. For negative A_t , the obtained bounds show a strong dependence on the value of ζ . The $\text{BR}(B_s \rightarrow \mu^+\mu^-)$ bounds in Fig. 6 clearly display the non-decoupling behavior mentioned above. Due to this non-decoupling, the $\text{BR}(B_s \rightarrow \mu^+\mu^-)$ results can constrain SUSY parameter space in regions that are beyond the current and expected future reach of direct searches.

A crucial element of our analysis is the viability of the cancellation of the SUSY contribution to the $B_s \rightarrow \mu^+\mu^-$ branching ratio. This cancellation is driven by the presence of ϵ_{FC} in (45), which is schematically given in (23) and its various contributions are detailed in (21), (25) and (26). First, in the following discussion, we neglect the wino contribution given by (26), which is generally smaller than the gluino contribution. This is due to the smallness of M_2 and α in (26) compared to M_3 and α_s in (25) (of course, our numerical analysis always includes the wino contribution). Since each SUSY contribution is proportional to μ , we see that switching the sign of μ changes the relative sign between the SUSY and SM amplitudes. Furthermore, by switching the sign of A_t , between the left and right panels of Fig. (6), we change the relative sign between the gluino contribution and the Higgsino contribution. Thus, for a particular choice of $\text{sign}(A_t)$ and $\text{sign}(\mu)$, we can exploit a cancellation between the gluino vs. Higgsino loop, diminishing the magnitude of the SUSY contribution, and a second cancellation between the overall SUSY contribution and the SM amplitude. In particular, even if the magnitude of the

SUSY contribution is by itself larger than the SM contribution, we can exercise the second cancellation where the SUSY amplitude overshoots the SM one.

These cancellations are clearly in effect in the left and right panels of Fig. 6. We first focus on the regions bounded by solid lines, which correspond to degenerate squark masses. This implies that the SUSY contribution dominantly arises from $\epsilon_b^{\tilde{H}}$ in (21). In the upper half of the left panel corresponding to positive A_t and positive μ , the SUSY contribution cancels with the SM contribution and always leads to a $\text{BR}(B_s \rightarrow \mu^+\mu^-)$ below the current bound. In the lower half of the left panel, with positive A_t and negative μ , the Higgsino contribution adds constructively with the SM contribution, leading to significant constraints. In the upper half of the right panel, the Higgsino contribution also adds constructively with the SM, leading again to a bound. This bound is less stringent compared to the positive A_t and negative μ case, because for positive μ , the ϵ_b and ϵ_0 terms in (45) lead to a suppression of the SUSY amplitude. Finally, in the lower half of the right panel, with negative A_t and negative μ , the Higgsino contribution interferes destructively with the SM. The constraint is non-vanishing, however, because for negative μ , the $\tan\beta$ resummation factors, given in (45), enhance the SUSY amplitude such that it can be more than twice as large as the SM amplitude.

When we include squark splitting, we further strengthen the SUSY contribution for positive A_t , because the gluino and Higgsino contributions add con-

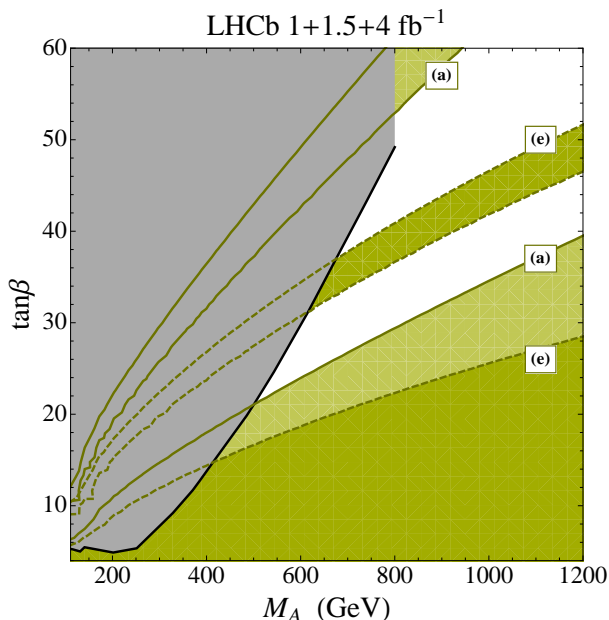


FIG. 7. The M_A - $\tan\beta$ plane in view of projected constraints from the $\text{BR}(B_s \rightarrow \mu^+\mu^-)$, assuming a future $\pm 0.5 \times 10^{-9}$ uncertainty in the measurement with the SM prediction as the central value. The green shaded regions between and below the solid and dashed contours correspond to values for $\tan\beta$ and M_A allowed in scenarios (a) and (e), as defined in Tab. I. The gray region is excluded by current direct searches of MSSM Higgs bosons in the $H/A \rightarrow \tau^+\tau^-$ channel.

structively. Hence the overall SUSY+SM interference is more restricted. The bounds due to this splitting in the masses are shown by the regions enclosed by the dashed and dotted lines in Fig. (6). For negative A_t , shown in the right panel, the gluino contribution partially cancels the Higgsino contribution, leading to a weaker constraint. The effect of the gluino contributions decreases for larger gluino mass, M_3 .

In tandem, the complementary views provided by the different panels of Figs. 5 and 6 clearly demonstrate that certain choices of SUSY parameters relax the constraints considerably. For example, with $M_A = 800$ GeV and $\tan\beta = 45$, the region of parameter space with positive μ and positive A_t is robustly unconstrained from the $B_s \rightarrow \mu^+\mu^-$ limit. Moving from top to bottom along a constant A_t contour in the left plot of Fig. 6 corresponds to a rapid coverage of the $\tan\beta$ vs. M_A plane from the (b) to (a) to (c) exclusion regions.

Regions of parameter space with destructive interference between SM and SUSY amplitudes (*i.e.* the regions with positive μA_t) will be constrained significantly if a lower bound of $\text{BR}(B_s \rightarrow \mu^+\mu^-)$ above half of the SM prediction is established in the future. We illustrate this in the plots of Figs. 7 and 8, which assume a measurement of $\text{BR}(B_s \rightarrow \mu^+\mu^-)$ at the SM expectation as a central value with an experimental uncertainty of $\pm 0.5 \times 10^{-9}$. Such a precision is expected to be achieved by LHCb at the end of the 13 TeV run with a combined analysis of

1 fb^{-1} of 7 TeV data, 1.5 fb^{-1} of 8 TeV data, and 4 fb^{-1} of 13 TeV data [186]. The plots in Figs. 7 and 8 show in green the regions in the M_A - $\tan\beta$ and m_{Q_3} - μ planes that are allowed by the expected results on the $B_s \rightarrow \mu^+\mu^-$ decay. As shown in Fig. 7, apart from the allowed regions with large M_A and small $\tan\beta$, there are also strips with large M_A and large $\tan\beta$ where the expected bounds from $B_s \rightarrow \mu^+\mu^-$ can be avoided. In these regions, the SUSY amplitude has approximately the same size as the SM amplitude but is opposite in sign. According to (44), this leads to a branching ratio close to the SM prediction.

For the example parameter point with $M_A = 800$ GeV and $\tan\beta = 45$, the projected lower bound on $\text{BR}(B_s \rightarrow \mu^+\mu^-)$ leads to very strong constraints in the m_{Q_3} - μ plane for positive μA_t . Indeed, for $M_A = 800$ GeV and $\tan\beta = 45$, and given the assumed experimental precision, charged Higgs loop contributions to $B_s \rightarrow \mu^+\mu^-$ already lead to a non-negligible suppression [187], leaving hardly any room for destructively interfering SUSY contributions. Only if the SUSY contribution is so large that $\mathcal{A} \simeq -1$ does the parameter space open up again. The corresponding regions that are excluded by the assumed lower bound are clearly visible in the white region of the upper half of the left plot and the upper white region in the lower half of the right plot in Fig. 8.

C. $B \rightarrow X_s \gamma$

The loop induced $B \rightarrow X_s \gamma$ decay is also highly sensitive to NP effects coming from SUSY particles. The NNLO SM prediction for the branching ratio reads [188] (see also [189, 190])

$$\text{BR}(B \rightarrow X_s \gamma)_{\text{SM}} = (3.15 \pm 0.23) \times 10^{-4}. \quad (46)$$

On the experimental side, BaBar recently presented updated results for the branching ratio [83]. Including this, the new world average reads [191]

$$\text{BR}(B \rightarrow X_s \gamma)_{\text{exp}} = (3.43 \pm 0.22) \times 10^{-4}, \quad (47)$$

which is slightly lower than the previous world average and is in very good agreement with the SM prediction. In the MSSM with minimal flavor violation and no new sources of CP violation, the branching ratio can be written as [192]

$$\begin{aligned} R_{bs\gamma} &= \frac{\text{BR}(B \rightarrow X_s \gamma)}{\text{BR}(B \rightarrow X_s \gamma)_{\text{SM}}}, \\ &\simeq 1 - 2.55 C_7^{\text{NP}} - 0.61 C_8^{\text{NP}} + 0.74 C_7^{\text{NP}} C_8^{\text{NP}} \\ &\quad + 1.57 (C_7^{\text{NP}})^2 + 0.11 (C_8^{\text{NP}})^2, \end{aligned} \quad (48)$$

where $C_{7,8}^{\text{NP}}$ are the NP contributions to the magnetic and chromo-magnetic $b \rightarrow s\gamma$ operators evaluated at the scale 160 GeV.

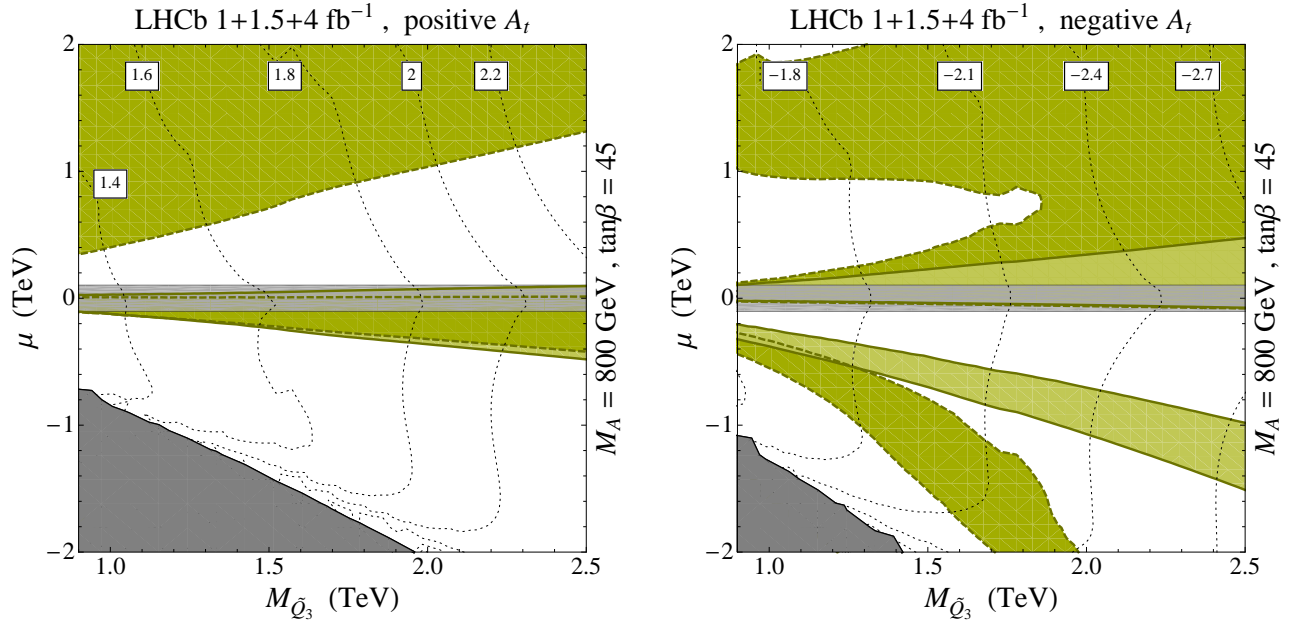


FIG. 8. The m_{Q_3} - μ plane in view of projected constraints from the $\text{BR}(B_s \rightarrow \mu^+ \mu^-)$, assuming a future $\pm 0.5 \times 10^{-9}$ uncertainty in the measurement with the SM prediction as the central value. We fixed $M_3 = 3M_2 = 6M_1 = 1.5$ TeV, $M_A = 800$ GeV and $\tan\beta = 45$. The green shaded regions between the solid contours correspond to values for m_{Q_3} and μ allowed for a degenerate squark spectrum. The green shaded regions between and above the dashed contours are allowed if the first two squark generations are 50% heavier than the third generation squark masses, with an alignment of $\zeta = 1$. The gray horizontal band corresponds to the constraint from direct searches of charginos at LEP. The vertical dotted lines show contours of constant A_t such that $M_h = 125$ GeV. In the gray regions in the lower left corners, the lightest Higgs mass is always below $M_h < 125$ GeV, taking into account a 3 GeV theory uncertainty.

Apart from the $B \rightarrow X_s \gamma$ decay, the modifications of the Wilson coefficients C_7 and C_8 also enter predictions of observables in the $B \rightarrow K^* \ell^+ \ell^-$ decay. In our MSSM setup with minimal flavor and CP violation, we only have real NP contributions to C_7 and C_8 . In this framework, the experimental data on $B \rightarrow K^* \ell^+ \ell^-$ does not put additional restrictions, once the bounds from $\text{BR}(B \rightarrow X_s \gamma)$ are taken into account [175, 193]. Therefore, we focus only on the $B \rightarrow X_s \gamma$ decay.

The SUSY contributions to $C_{7,8}^{\text{NP}}$ come from charged Higgs-top loops, neutral Higgs-bottom loops, Higgsino-stop loops, and gaugino-squark loops. As with the Higgs-fermion couplings, we take into account the most generic MFV structure of the squark masses and consistently consider splittings between the first two and the third generation squarks in the left-handed as well as the right handed sector. The resulting dominant MSSM contributions to $C_{7,8}$ read

$$C_{7,8}^H = \left(\frac{1 - \epsilon'_0 t_\beta}{1 + \epsilon_b t_\beta} + \frac{\epsilon'_{\text{FC}} \epsilon_{\text{FC}} t_\beta^2}{(1 + \epsilon_b t_\beta)(1 + \epsilon_0 t_\beta)} \right) \frac{m_t^2}{2M_{H^\pm}^2} h_{7,8}(r_t) + \frac{\epsilon_{\text{FC}} t_\beta^3}{(1 + \epsilon_b t_\beta)^2 (1 + \epsilon_0 t_\beta)} \frac{m_b^2}{2M_A^2} z_{7,8}, \quad (49)$$

$$C_{7,8}^{\tilde{H}} = -\frac{t_\beta}{1 + \epsilon_b t_\beta} \frac{m_t^2}{2} A_t \mu f_{7,8}^{\tilde{H}}(m_{Q_3}^2, m_{U_3}^2, \mu^2), \quad (50)$$

$$\begin{aligned} \frac{g_2^2}{g_3^2} C_{7,8}^{\tilde{g}} &= \frac{t_\beta}{1 + \epsilon_0 t_\beta} M_W^2 \mu M_3 \zeta \left(f_{7,8}^{\tilde{g}}(m_{Q_3}^2, m_{D_3}^2, M_3^2) - f_{7,8}^{\tilde{g}}(m_{Q_3}^2, m_{D_3}^2, M_3^2) \right) \\ &\quad - \frac{\epsilon_{\text{FC}} t_\beta^2}{(1 + \epsilon_b t_\beta)(1 + \epsilon_0 t_\beta)} M_W^2 \mu M_3 f_{7,8}^{\tilde{g}}(m_{Q_3}^2, m_{D_3}^2, M_3^2), \end{aligned} \quad (51)$$

$$\begin{aligned} C_{7,8}^{\tilde{W}} &= \frac{t_\beta}{1 + \epsilon_0 t_\beta} M_W^2 \mu M_2 \zeta \left(f_{7,8}^{\tilde{W}}(M_2^2, \mu^2, m_{Q_3}^2) - f_{7,8}^{\tilde{W}}(M_2^2, \mu^2, m_{Q_3}^2) \right) \\ &\quad - \frac{\epsilon_{\text{FC}} t_\beta^2}{(1 + \epsilon_b t_\beta)(1 + \epsilon_0 t_\beta)} M_W^2 \mu M_2 f_{7,8}^{\tilde{W}}(M_2^2, \mu^2, m_{Q_3}^2). \end{aligned} \quad (52)$$

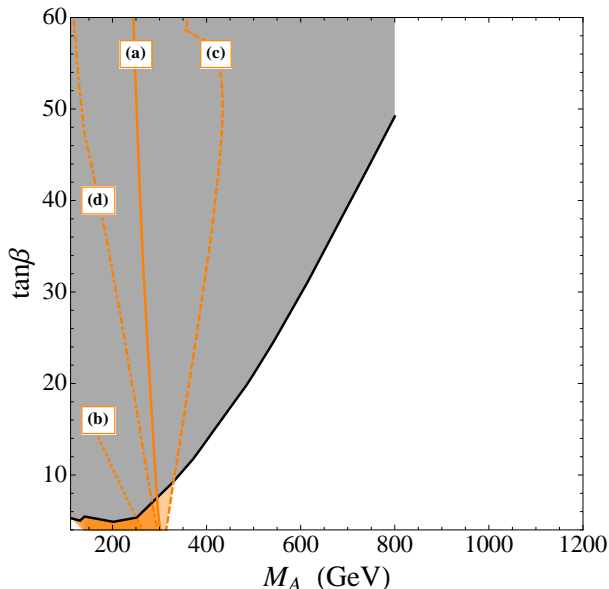


FIG. 9. Constraints in the M_A - $\tan\beta$ plane from the $B \rightarrow X_s\gamma$ decay. The orange solid, dotted, dashed, and dash-dotted contours correspond to scenarios (a), (b), (c), and (d) as described in the text. The gray region is excluded by direct searches of MSSM Higgs bosons in the $H/A \rightarrow \tau^+\tau^-$ channel.

The first term in (49) corresponds to contributions from a charged Higgs loop. The loop functions, $h_{7,8}$ depend on the ratio of the top mass and the charged Higgs mass, $r_t = m_t^2/M_{H^\pm}^2$, and for $r_t = 1$ are given by $h_7(1) = -7/18$ and $h_8(1) = -1/3$. Their full analytical expressions can be found in the appendix. The second term in (49) arises from neutral heavy Higgs loops. It is strongly suppressed by the bottom quark mass and is only important for very large $\tan\beta$. The loop functions, $z_{7,8}$, depend on the ratio of the bottom mass and the charged Higgs mass and since $m_b^2/M_{H^\pm}^2 \ll 1$, they are very well approximated by $z_7 = -\frac{1}{18}$ and $z_8 = \frac{1}{6}$.

Contributions from Higgsino-stop, gluino-down squark, and Wino-down squark loops are shown in (50), (51), and (52), respectively. We do not write the typically negligible bino contributions.

For a degenerate SUSY spectrum with mass \tilde{m} , the loop functions entering the Higgsino and gaugino contributions reduce to

$$\begin{aligned} f_7^{\tilde{H}} &\rightarrow \frac{5}{36} \frac{1}{\tilde{m}^4}, & f_7^{\tilde{g}} &\rightarrow -\frac{2}{27} \frac{1}{\tilde{m}^4}, & f_7^{\tilde{W}} &\rightarrow -\frac{7}{24} \frac{1}{\tilde{m}^4}, \\ f_8^{\tilde{H}} &\rightarrow \frac{1}{12} \frac{1}{\tilde{m}^4}, & f_8^{\tilde{g}} &\rightarrow -\frac{5}{18} \frac{1}{\tilde{m}^4}, & f_8^{\tilde{W}} &\rightarrow -\frac{1}{8} \frac{1}{\tilde{m}^4}. \end{aligned}$$

Their full analytical expressions are collected in the appendix. In contrast to the Higgs penguin contributions to $B_s \rightarrow \mu^+\mu^-$, the SUSY loop contributions to $b \rightarrow s\gamma$ do decouple with the SUSY scale.

The first terms in (51) and (52) correspond to 1-loop flavor changing gaugino contributions. They vanish for

$m_{Q_3} = m_Q$, *i.e.* if there is no splitting between the first two and the third generations of left-handed squark masses. In the presence of a splitting, the parameter ζ again parametrizes the alignment of the left-handed squark mass matrix. As mentioned before, if the splitting is generated by RGE running we expect $1/2 < \zeta < 1$. The second terms in (51) and (52) are formally 2-loop contributions but they can be relevant for large $\tan\beta$. They *do not* vanish for degenerate masses [110, 143].

Similarly to $B_s \rightarrow \mu^+\mu^-$, the MSSM contribution to $B \rightarrow X_s\gamma$ is a sum of several terms that depend sensitively on many parameters, particularly the signs of μ and A_t .

In Fig. 9, we show in orange the constraints from $B \rightarrow X_s\gamma$ in the M_A - $\tan\beta$ plane obtained analogous to the $B_s \rightarrow \mu^+\mu^-$ constraints discussed previously. The plots of Fig. 10 show the $B \rightarrow X_s\gamma$ constraints in the plane of the third generation squark masses and the Higgsino mass parameter μ , again in complete analogy to the $B_s \rightarrow \mu^+\mu^-$ constraints.

We can again see the connection between the constraints in the $\tan\beta$ vs. M_A plane, given in Fig. 9, and the μ vs. m_{Q_3} plane, given in Fig. 10. The squark masses are fixed to 2 TeV in Fig. 9. This causes the stop-chargino contribution to be essentially negligible, and hence we are only constrained by the Higgs contribution in the low M_A and large $\tan\beta$ regions. For heavy squarks and low $\tan\beta$, the bound on the charged Higgs mass is approximately independent of the other SUSY parameters and is given by $M_{H^\pm} \gtrsim 300$ GeV. For large $\tan\beta$, the resummation factors in (49) become relevant. The most important effect arises from the factors ϵ'_0 and ϵ_b in the first term in (49). For negative μ , ϵ'_0 and ϵ_b are negative and therefore the bounds become stronger for larger $\tan\beta$ in scenario (c). For positive μ (scenarios a, b, and d) instead, the bounds are relaxed for large $\tan\beta$. As the dominant gluino contribution to ϵ'_0 and ϵ_b grows with μ the $B \rightarrow X_s\gamma$ constraint is weakest in scenario (b) that has the largest $\mu = 4$ TeV. For the heavy squark masses chosen in Fig. 9, the direct searches for MSSM Higgs bosons give stronger constraints compared to $B \rightarrow X_s\gamma$ except for small values of $\tan\beta$.

In the plots of Fig. 10, the variation of the squark masses allows the stop-chargino contribution to become important for small m_{Q_3} , demonstrating that the $\tan\beta$ vs. M_A projection insufficiently illustrates the $B \rightarrow X_s\gamma$ constraint. Partial cancellations are again in effect, and we describe the relative signs of the various contributions in the following. Apart from extreme regions of parameter space, the charged Higgs contribution interferes constructively with the SM and enhances $\text{BR}(B \rightarrow X_s\gamma)$. However, for the case shown, $M_A = 800$ GeV, this contribution is small. For positive (negative) (μA_t) , the Higgsino loop contribution come with same (opposite) sign with respect to the SM. Among the gaugino contributions, the dominant one is typically the 1-loop gluino contribution. If a splitting in the left-handed squark masses is induced radiatively, its sign depends, for positive M_3 ,

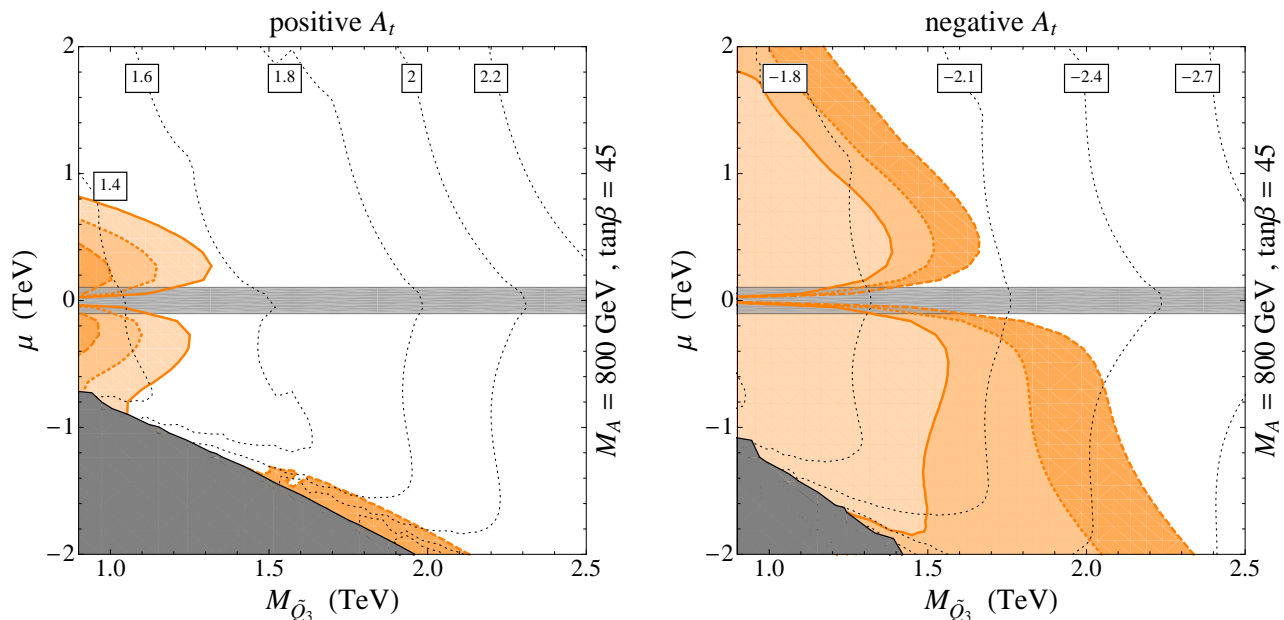


FIG. 10. Constraints in the m_{Q_3} - μ plane from the $B \rightarrow X_s \gamma$ decay, for fixed $M_3 = 3M_2 = 6M_1 = 1.5$ TeV. The solid bounded regions correspond to a degenerate squark spectrum. The dashed and dotted bounded regions correspond to choosing the first two squark generations 50% heavier than the third generation squark masses, with an alignment of $\zeta = 1$ and $\zeta = 0.5$, respectively. The gray horizontal band corresponds to the constraint from direct searches of charginos at LEP. The vertical dotted lines show contours of constant A_t such that $M_h = 125$ GeV. In the gray regions in the lower left corners the lightest Higgs mass is always below $M_h < 125$ GeV, taking into account a 3 GeV theory uncertainty.

only on the sign of μ . For positive (negative) μ , gluinos interfere destructively (constructively) with the SM.

The plots of Fig. 10 clearly show the decoupling behavior of the MSSM contributions to the $b \rightarrow s \gamma$ transition. For a degenerate squark spectrum ($m_{Q_3} = m_Q = m_{U_3} = m_U = m_{D_3} = m_D = \tilde{m}$) and a heavy charged Higgs, the bound from $\text{BR}(B \rightarrow X_s \gamma)$ hardly constrains the MSSM parameter space beyond squark masses that are already excluded by direct SUSY searches, namely $\tilde{m} \gtrsim \mathcal{O}(1 \text{ TeV})$. In the presence of a mass splitting between the first two and the third generations of squarks, the $B \rightarrow X_s \gamma$ constraint can become relevant for negative A_t , since the gluino and Higgsino contributions add constructively. Squark masses significantly above 1 TeV can be probed in that case. For positive values of A_t , on the other hand, the gluino and Higgsino loops partially cancel and the bound from $B \rightarrow X_s \gamma$ is barely relevant.

D. Discussion of RGE Effects

Our phenomenological analysis of MSSM mass parameters serves our purpose of understanding the flavor constraints on the low energy MSSM spectrum. However, we also want to connect these constraints to parameters of a high scale SUSY parameter space. To this end, we consider a typical example in the large $\tan\beta$ and M_A region compatible with direct $H/A \rightarrow \tau^+ \tau^-$ searches at the LHC. We show typical mass differences

between soft parameters for squarks in the plane of the mSUGRA boundary conditions, m_0 and $m_{1/2}$, fixing the remaining mSUGRA parameters to $A_0 = \pm 2$ TeV and $\tan\beta = 45$. We also chose the SUSY breaking scale to be the GUT scale, 10^{16} GeV. We deviate slightly from the strict mSUGRA prescription and work in a non-universal Higgs mass (NUHM) scenario by fixing the Higgs soft mass $m_{H_u}^2 = 1 \text{ TeV}^2$ and adjusting $m_{H_d}^2$ at the high scale to obtain M_A within 10% of 800 GeV at the low scale of $Q = 1$ TeV. Using these boundary conditions and the usual low energy Yukawa constraints derived from fermion masses run to $Q = 1$ TeV, we numerically solve the RGE system dictated by 2-loop running from [194] and 1-loop radiative corrections from [195]. Our choice of A_0 typically gives the lightest SM-like Higgs a mass of 122 ± 2 GeV. For the bulk of the region in the $(m_0, m_{1/2})$ plane, adjusting A_0 (in particular, A_t) to obtain a Higgs mass of 125 GeV changes the quantitative picture by less than a few percent. For very small m_0 and $m_{1/2}$, however, where some squarks or sleptons become close to tachyonic, the mass splittings can vary significantly as result of changing A_0 .

We highlight that the B observable constraints can vary significantly as a result of Yukawa-induced squark mass splittings inherent in RG running, as seen in Fig. 6 and Fig. 10, respectively. In particular, the most significant mass splittings among the squarks occur as a result of the top and bottom Yukawas, where a significant enhancement of the bottom Yukawa occurs for large $\tan\beta$.

We can obtain a semi-analytic understanding of the re-

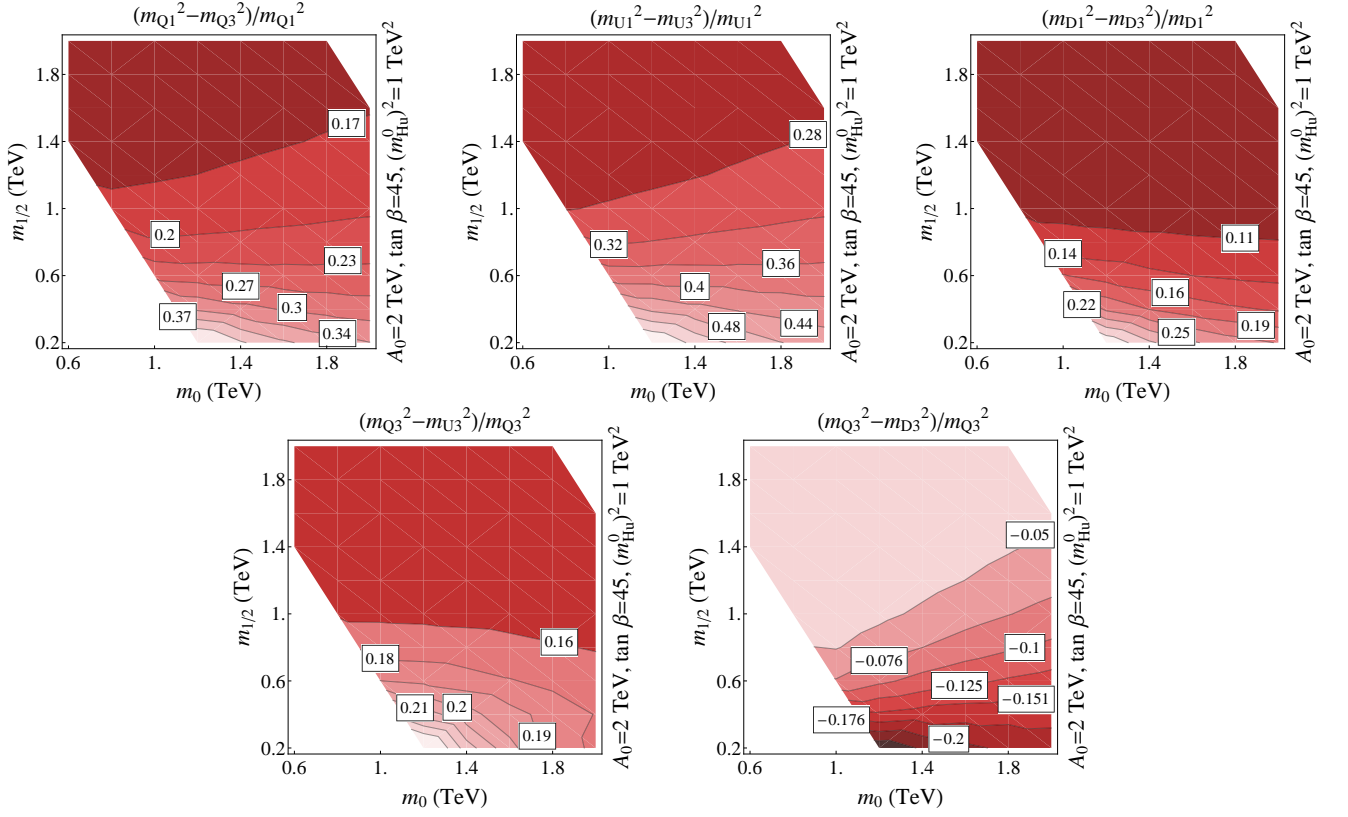


FIG. 11. Contours of ΔQ_{13} (top left), ΔU_{13} (top middle), ΔD_{13} (top right), ΔQU_3 (bottom left), and ΔQD_3 (bottom right) in the $(m_0, m_{1/2})$ plane, fixing $A_0 = 2$ TeV, $(m_{H_u}^0)^2 = 1$ TeV², $\tan \beta = 45$, and requiring $M_A = 800$ GeV within 10%.

sulting mass splittings, following the simplified 1-loop RG analysis of [196–198]. Neglecting the first- and second-generation Yukawa couplings and α_1^2 contributions, we have

$$m_{Q_3}^2(t) \approx m_{Q_3}^2(0) + I_{\alpha_3} + I_{\alpha_2} - I_t - I_b, \quad (53)$$

$$m_{U_3}^2(t) \approx m_{U_3}^2(0) + I_{\alpha_3} - 2I_t, \quad (54)$$

$$m_{D_3}^2(t) \approx m_{D_3}^2(0) + I_{\alpha_3} - 2I_b, \quad (55)$$

and

$$I_{\alpha_3} \equiv \int dt \left(\frac{16}{3} \frac{\alpha_3}{4\pi} M_3^2 \right), \quad (56)$$

$$I_{\alpha_2} \equiv \int dt \left(3 \frac{\alpha_2}{4\pi} M_2^2 \right), \quad (57)$$

$$I_t \equiv \frac{1}{16\pi^2} \int dt y_t^2 (m_Q^2 + m_U^2 + m_{H_u}^2 + A_t^2), \quad (58)$$

$$I_b \equiv \frac{1}{16\pi^2} \int dt y_b^2 (m_Q^2 + m_D^2 + m_{H_d}^2 + A_b^2), \quad (59)$$

where $t = 0$ corresponds to the GUT scale. The analogous $m_{Q_1}^2$, $m_{U_1}^2$, and $m_{D_1}^2$ approximations can be obtained from the above by neglecting the I_t and I_b contributions.

For the trilinear couplings, neglecting α_1 and A_τ ,

$$A_t \approx A_0 + \int dt \left[\left(\frac{16}{3} \frac{\alpha_3}{4\pi} M_3 + 3 \frac{\alpha_2}{4\pi} M_2 \right) \right.$$

$$\left. - 6 \frac{y_t^2}{16\pi^2} A_t - \frac{y_b^2}{16\pi^2} A_b \right] \quad (60)$$

$$A_b \approx A_0 + \int dt \left[\left(\frac{16}{3} \frac{\alpha_3}{4\pi} M_3 + 3 \frac{\alpha_2}{4\pi} M_2 \right) \right. \\ \left. - \frac{y_t^2}{16\pi^2} A_t - 6 \frac{y_b^2}{16\pi^2} A_b \right]. \quad (61)$$

The most relevant mass splittings for our analysis are

$$\Delta Q_{13} \equiv \frac{m_{Q_1}^2 - m_{Q_3}^2}{m_{Q_1}^2} \approx \frac{I_t + I_b}{m_{Q_1}^2} \quad (62)$$

$$\Delta U_{13} \equiv \frac{m_{U_1}^2 - m_{U_3}^2}{m_{U_1}^2} \approx \frac{2I_t}{m_{U_1}^2} \quad (63)$$

$$\Delta D_{13} \equiv \frac{m_{D_1}^2 - m_{D_3}^2}{m_{D_1}^2} \approx \frac{2I_b}{m_{D_1}^2} \quad (64)$$

$$\Delta QU_3 \equiv \frac{m_{Q_3}^2 - m_{U_3}^2}{m_{Q_3}^2} \approx \frac{I_{\alpha_2} + I_t - I_b}{m_{Q_1}^2 - I_t - I_b} \quad (65)$$

$$\Delta QD_3 \equiv \frac{m_{Q_3}^2 - m_{D_3}^2}{m_{Q_3}^2} \approx \frac{I_{\alpha_2} - I_t + I_b}{m_{Q_1}^2 - I_t - I_b}. \quad (66)$$

From these relations we see that $\Delta U_{13} + \Delta D_{13} \approx 2\Delta Q_{13}$, where ΔD_{13} is small compared to ΔU_{13} for small $\tan \beta$. We also expect $\Delta QU_3 = -\Delta QD_3$ for small $m_{1/2}$. These relations for the various mass splittings, based on 1-loop

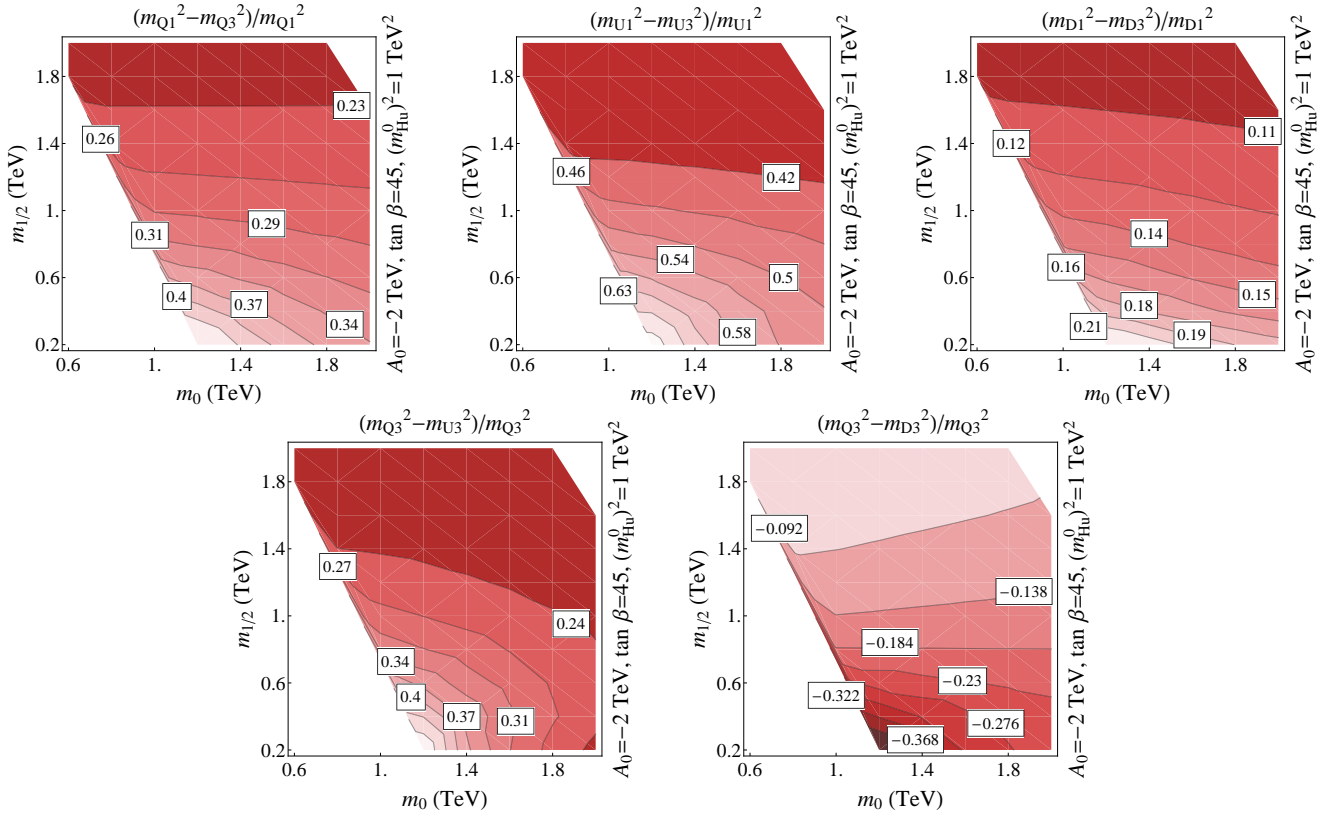


FIG. 12. Same as Fig. 11 except $A_0 = -2$ TeV.

semi-analytic results, are borne out in our numerical results, which are calculated from 2-loop RG running, and are shown in Fig. 11 and Fig. 12.

For a gluino with mass $M_3 = 1.5$ TeV as we considered in the previous sections, we have $m_{1/2} \simeq 500$ GeV and therefore a significant splitting is induced among the squark masses in running down from the GUT scale. The most important splitting in the general discussion of the previous sections is ΔQ_{13} , as it leads to gaugino loop contributions to FCNCs. In our mSUGRA setup, it is typically around 25% for positive A_0 and 35% for negative A_0 . The splitting between the masses of the squarks decreases for larger $m_{1/2}$. This is due to the universal $SU(3)$ contribution, I_{α_3} , to m_{Q_3} , m_Q , m_{U_3} , m_U , m_{D_3} , and m_D , which dominates for large $m_{1/2}$.

From the approximate expressions above, we can also estimate the size of ζ resulting from running. We have

$$\zeta \simeq \frac{I_t}{I_t + I_b}. \quad (67)$$

Even though we chose a large value of $\tan \beta = 45$ for the examples shown, the bottom Yukawa effects are limited. Note that for the parameter region explored here, $\zeta \sim 80\%$, which means that the squark mass splitting is dominantly driven by the top Yukawa and therefore aligned in the up-sector. For smaller $\tan \beta$, the alignment parameter ζ is even closer to 1.

Note that the gaugino loop contributions to FCNCs

depend approximately on the product $\zeta \times \Delta Q_{13}$. In the mSUGRA scenario discussed here, we find to a good approximation $\zeta \times \Delta Q_{13} \simeq \Delta U_{13}/2$. In more generic setups however, this relation does not hold and we will continue to discuss the gaugino loop contributions to FCNCs in terms of ζ and ΔQ_{13} separately.

In the plots of Fig. 13, we show again the constraints from $B_s \rightarrow \mu^+ \mu^-$ and $B \rightarrow X_s \gamma$ in the $m_{Q_3} - \mu$ plane, this time setting the various mass splittings according to our results of the mSUGRA RGE running. In particular, we use $\Delta Q_{13} = 0.35$, $\Delta U_{13} = 0.6$, $\Delta D_{13} = 0.15$, $\Delta Q U_3 = 0.35$, and $\Delta Q D_3 = -0.25$, which are typical values for $m_{1/2} \simeq 500$ GeV and negative A_t . As we saw in the previous sections for positive A_t , the $B_s \rightarrow \mu^+ \mu^-$ constraint depends very mildly on the squark mass splitting and the $B \rightarrow X_s \gamma$ constraint is barely relevant. Therefore, we restrict ourselves to negative A_t . For comparison, the solid contours indicate again the constraints obtained for a degenerate squark spectrum. The dotted contours corresponds to keeping all third generation squarks degenerate and only implementing the splitting between the first two and the third generation as given by the RGE running. The dashed contours correspond to the situation where all squark mass splittings are as dictated by the RGE running. The former case behaves as expected given the analysis of Secs. VB and VC. For the latter case, however, once mass splittings between the different types of third generation squarks are also

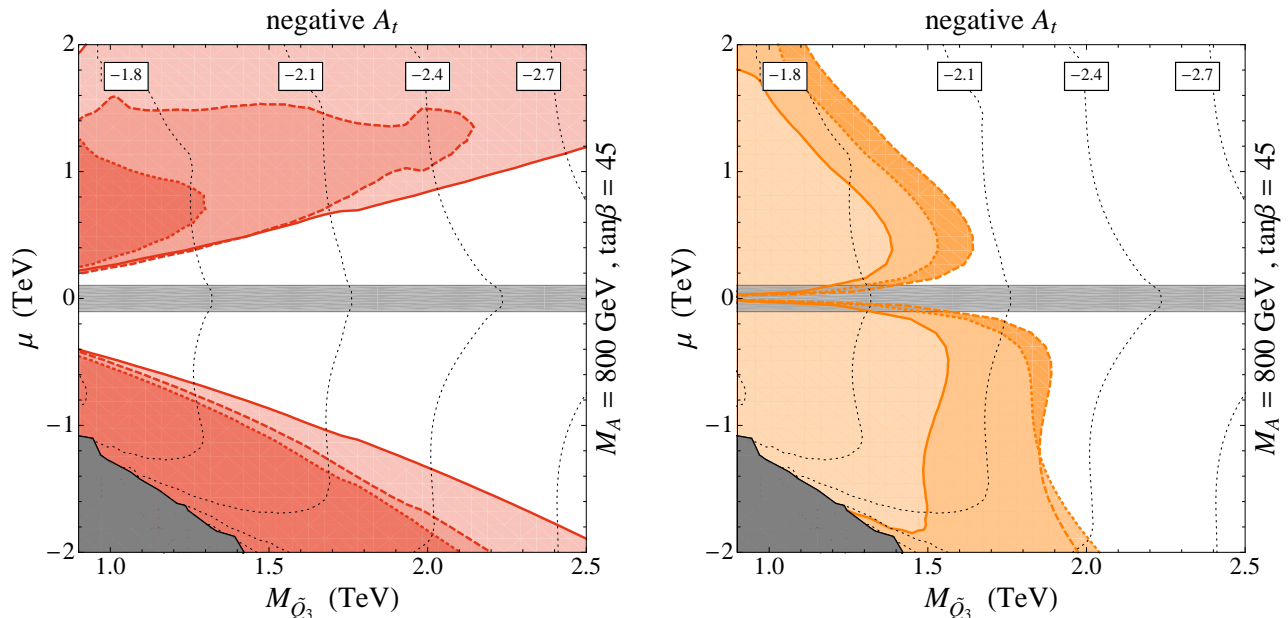


FIG. 13. Constraints in the m_{Q_3} - μ plane from $B_s \rightarrow \mu^+\mu^-$ (left) and $B \rightarrow X_s\gamma$ (right). The solid bounded regions correspond to a degenerate squark spectrum. The dashed and dotted bounded regions correspond to mass splittings in the squark spectrum implied by RGE running. In particular $\Delta Q_{13} = 0.35$, $\Delta U_{13} = 0.6$, $\Delta D_{13} = 0.15$, $\Delta QU_3 = 0.35$, and $\Delta QD_3 = -0.25$ for the dashed contours and $\Delta Q_{13} = 0.35$, $\Delta U_{13} = 0.6$, $\Delta D_{13} = 0.15$, and $\Delta QU_3 = \Delta QD_3 = 0$ for the dotted contours. The gray horizontal band corresponds to the constraint from direct chargino searches. The vertical dotted lines show contours of constant A_t such that $M_h = 125$ GeV. In the gray regions in the lower left corners the lightest Higgs mass is always below $M_h < 125$ GeV, taking into account a 3 GeV theory uncertainty.

considered, an additional effect arises. As can be seen from (54) and confirmed in the lower left plots of Figs. 11 and 12, the right handed stop is typically significantly lighter than the other third generation squarks. The light right-handed stop then increases the chargino-stop loop contributions to $B_s \rightarrow \mu^+\mu^-$ and to $B \rightarrow X_s\gamma$ leading overall to stronger constraints compared to the case of degenerate third generation squarks.

Two of the most important quantities dictated by RGEs for flavor observables are the values of ΔQ_{13} and ζ . Within the assumption of flavor universality at the messenger scale, ΔQ_{13} and ζ depend mainly on the messenger scale, $\tan\beta$ and the ratio of gluino mass to squark masses. Lowering the messenger scale from the GUT scale as well as increasing the gluino mass decreases the splitting ΔQ_{13} , but leaves ζ approximately invariant. Smaller (larger) values of $\tan\beta$ would decrease (increase) ΔQ_{13} and simultaneously increase (decrease) ζ , leaving the product $\zeta \times \Delta Q_{13} \simeq \Delta U_{13}/2$ approximately invariant. As we saw, making the splitting smaller strengthens the $\text{BR}(B_s \rightarrow \mu^+\mu^-)$ constraint for negative A_t , but increasing ζ will relax it. The effect of these two quantities is exactly opposite on the constraints coming from $\text{BR}(B \rightarrow X_s\gamma)$. This complimentary behavior implies that even varying the messenger scale and $\tan\beta$, these two flavor observables will be able to constrain the parameter space efficiently.

VI. DARK MATTER DIRECT DETECTION

The lightest neutralino in the MSSM is an excellent thermal dark matter candidate. The lightest neutralino is a weakly interacting massive particle (WIMP) and therefore generically leads to roughly the correct order of magnitude for the observed dark matter relic density. This is particularly true in the well-tempered neutralino scenario [199], where the lightest neutralino is a mixture of the Bino and Wino or the Higgsino. In the following we do not assume any specific mechanism by which the correct dark matter relic abundance is achieved, but simply assume that the lightest neutralino in the MSSM accounts for the dark matter in the universe [200].

Neutralinos interact with SM matter and therefore dark matter direct detection limits can be used to put bounds on the MSSM parameter space, complementary to the bounds from direct searches and low energy flavor observables [59, 68, 201–209].

The Xenon100 Collaboration recently set very stringent limits on the spin-independent elastic dark matter nucleon scattering cross section [84, 211]. For dark matter masses of $\mathcal{O}(100 \text{ GeV})$, the bounds are as strong as $\sigma < 2 \times 10^{-45} \text{ cm}^2$, assuming canonical values for the local dark matter density, the local circular velocity and the Galactic escape velocity. Interpreted in the context of the MSSM with neutralino dark matter, these bounds are starting to probe significant parts of the parameter

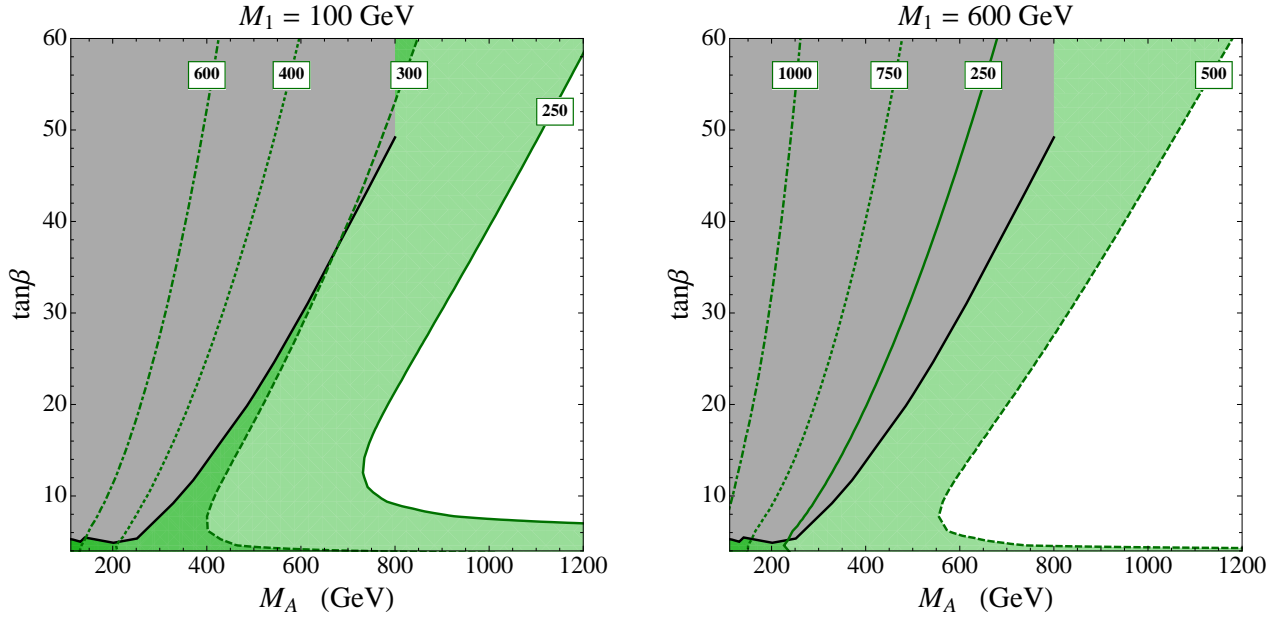


FIG. 14. Constraints in the M_A - $\tan\beta$ plane from Dark Matter direct detection. The green solid, dashed, dotted and dash-dotted contours correspond to different values of μ as indicated. The gray region is excluded by direct searches of MSSM Higgs bosons in the $H/A \rightarrow \tau^+\tau^-$ channel.

space.

The spin-independent elastic neutralino-proton cross-section can be written as

$$\sigma = \frac{4M_\chi^2 m_p^2}{\pi(M_\chi + m_p)^2} f_p^2, \quad (68)$$

where M_χ is the mass of the lightest neutralino, m_p is the proton mass, and

$$\frac{f_p}{m_p} = \left(\sum_{q=u,d,s} f_{T_q}^p c_q + \frac{2}{27} f_{TG}^p \sum_{q=c,b,t} c_q \right). \quad (69)$$

The non-perturbative parameters $f_{T_q}^p$ and $f_{TG}^p = 1 - f_{T_u}^p - f_{T_d}^p - f_{T_s}^p$ come from the evaluation of nuclear matrix elements. We use the latest lattice determinations in our numerical analysis [210]

$$f_{T_u}^p = f_{T_d}^p = 0.028, \quad f_{T_s}^p = 0.0689. \quad (70)$$

These values are expected to be affected by considerable uncertainties. We assume isospin symmetry when applying the Xenon100 bounds.

For large $\tan\beta$, the dominant contributions to the coefficients, c_q , parametrizing the neutralino-quark couplings, typically come from the t -channel exchange of the heavy scalar H and read

$$c_d^H = c_s^H \simeq \frac{g_1^2}{4M_H^2} \frac{t_\beta}{1 + \epsilon_s t_\beta} \frac{\mu}{M_1^2 - \mu^2}, \quad (71)$$

$$c_b^H \simeq \frac{g_1^2}{4M_H^2} \frac{t_\beta}{1 + \epsilon_b t_\beta} \frac{\mu}{M_1^2 - \mu^2}. \quad (72)$$

The t -channel exchange of the SM-like Higgs affects all c_q approximately equally:

$$c_q^h \simeq \frac{g_1^2}{4M_h^2} \frac{M_1}{M_1^2 - \mu^2}. \quad (73)$$

While the c_q^h are not enhanced by $\tan\beta$, bounds on the direct detection cross section have become so strong that the t -channel exchange of the SM-like Higgs is also probed.

The above expressions hold in the large $\tan\beta$ limit and assume the lightest supersymmetric particle to be mainly a bino-higgsino mixture with $M_1 \neq \mu$. In our numerical analysis, we go beyond the large $\tan\beta$ limit: we work with neutralino mass eigenstates and include the effects from s -channel squark exchange, though these are always very suppressed by the squark masses.

As is evident from (71), (72), and (73), the neutralino-proton cross section depends strongly on M_1 and μ . This can be also seen from the plots of Fig. 14, which show in green the regions in the canonical M_A - $\tan\beta$ plane that are excluded by the Xenon100 constraints. In the left plot, the bino mass is set to $M_1 = 100$ GeV with $M_2 = 2M_1$ and the solid, dashed, dotted and dash-dotted contours correspond to $\mu = 250$ GeV, 300 GeV, 400 GeV, and 600 GeV, as indicated in the plot. In the right plot, we choose a larger bino mass of $M_1 = 600$ GeV, with $M_2 = 2M_1$ again, and the solid, dashed, dotted and dash-dotted contours correspond to $\mu = 250$ GeV, 500 GeV, 750 GeV, and 1000 GeV. Dependence on other SUSY parameters enters at the loop level through the ϵ_i factors in (71) and (72) and is therefore very moderate. In these plots we fix a common squarks mass, $\tilde{m} = 2$ TeV,

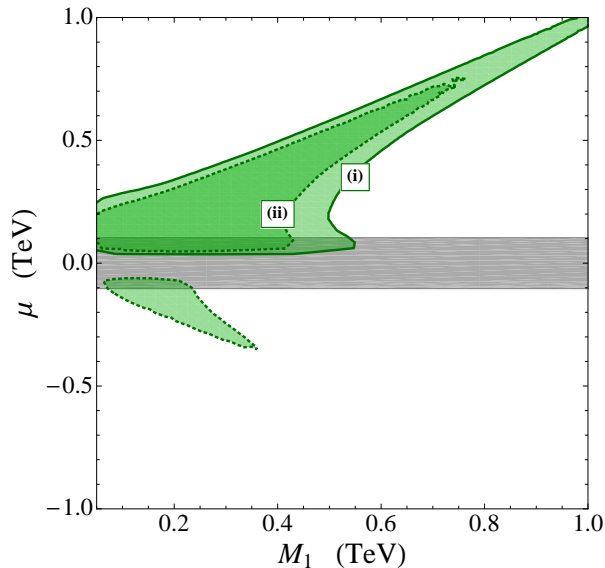


FIG. 15. Constraints in the M_1 - μ plane from Dark Matter direct detection. The solid and dashed contours correspond to different choices for M_A and $\tan\beta$ as defined in the text. The horizontal gray band is excluded by direct chargino searches.

a gluino mass of $M_3 = 1.5$ TeV and $A_t = A_b = A_\tau$ such that the lightest Higgs mass 125 GeV.

The strongest constraints arise if bino and higgsinos are maximally mixed, *i.e.* for $M_1 \simeq \mu$. Indeed, if $M_1 = \mu$, we find, independent of the values of M_A and $\tan\beta$, that the exchange of the SM-like Higgs leads to direct detection cross sections that are already ruled out by the current bounds in the full range of neutralino masses up to 1 TeV. Away from bino-higgsino degeneracy, regions of parameter space open up. Still, for small heavy Higgs masses and large values of $\tan\beta$, the heavy Higgs exchange contributions can be sizable and lead to important constraints in the M_A - $\tan\beta$ plane, as long as μ and $M_1 \lesssim 1$ TeV. In the excluded regions with small $\tan\beta$ and a large heavy Higgs mass, the constraint arises from the exchange of the light Higgs.

The plot of Fig. 15 shows the direct detection constraints in the M_1 - μ plane for 2 different points in the M_A - $\tan\beta$ plane. The solid, dashed and dotted contours correspond to $M_A = 800$ GeV and $\tan\beta = 45$ (scenario i) and $M_A = 1$ TeV and $\tan\beta = 10$ (scenario ii), both compatible with current direct searches. As already mentioned, the strongest constraints arise along the $M_1 \simeq \mu$ line. Interestingly, the constraints for negative values of μ are considerably weaker, because for negative μ , the heavy Higgs and SM like Higgs contributions interfere destructively. Observe that this behavior is opposite to that of the constraints coming from $B_s \rightarrow \mu^+\mu^-$ and $B \rightarrow X_s\gamma$, which are currently weaker for positive μ (and positive A_t).

Note that the bounds from dark matter direct detection not only depend very strongly on various MSSM pa-

rameters, but are also affected by various uncertainties, *e.g.* from the nuclear matrix elements, and astrophysical uncertainties, in particular the dark matter velocity distribution. Moreover, they also depend crucially on the assumption that the dark matter of the universe indeed consist entirely of MSSM neutralinos. If neutralinos only make up a (small) fraction of the dark matter, the bounds can be relaxed considerably and even avoided completely.

VII. CONCLUSIONS

In this work, we evaluated the status of the minimal supersymmetric standard model with minimal flavor violation in light of the recent Higgs discovery as well as constraints from collider searches, flavor measurements, and dark matter direct detection experiments. In concert, these complementary probes provide valuable constraints on the MSSM parameter space. In particular, we showed that flavor bounds can be stronger than bounds from direct searches for heavy MSSM Higgs particles or supersymmetric particles, even in the restrictive framework of MFV.

Throughout our analysis, we consistently implemented the most general structure of the soft SUSY breaking terms compatible with the MFV ansatz, *i.e.* allowing splitting between the first two and the third generations of squarks. We demonstrated that, in addition to the typical pMSSM parameters, an additional parameter, ζ , reflective of the alignment of the mass splitting of the left-handed squarks, is required to discuss the flavor phenomenology of this framework. In the presence of such splitting, this parameter controls the size of gaugino-squark loop contributions to FCNCs. Possible cancellations between gaugino and higgsino loop contributions have a very strong dependence on ζ . We showed its impact in the $B_s \rightarrow \mu^+\mu^-$ and $B \rightarrow X_s\gamma$ decays and presented expectations for its magnitude as dictated by RGE running.

We discussed the constraints from direct searches of the heavy MSSM Higgs bosons. Bounds from $H/A \rightarrow \tau^+\tau^-$ searches mainly depend on M_A and $\tan\beta$ and are robust against variations of other SUSY parameters. Separately, searches in the $H/A \rightarrow b\bar{b}$ channel show a stronger dependence on the parameters under consideration, in particular on the sign and magnitude of the Higgsino mass parameter, μ , and therefore provide complementary information. Currently, however, the $H/A \rightarrow \tau^+\tau^-$ searches are more strongly constraining for the considered scenarios.

On the flavor side, we considered the tree level decay $B \rightarrow \tau\nu$ as well as the loop induced FCNC processes $B_s \rightarrow \mu^+\mu^-$ and $B \rightarrow X_s\gamma$. The recent experimental updates on the $\text{BR}(B \rightarrow \tau\nu)$ show reasonable agreement with the SM prediction. At tree level, charged Higgs contributions to $B \rightarrow \tau\nu$ interfere destructively with the SM amplitude. At the loop level, a net constructive interference is in principle possible for very large

and negative $\mu \tan \beta$. However, we find that the corresponding regions of parameter space are excluded by vacuum meta-stability considerations. The $B \rightarrow \tau \nu$ decay can lead to constraints in the M_A - $\tan \beta$ plane also for $M_A > 800$ GeV where current direct searches for MSSM Higgs bosons end. For such heavy Higgs bosons however, $B \rightarrow \tau \nu$ only probes very large values of $\tan \beta \gtrsim 60$. The $B \rightarrow \tau \nu$ constraints depend only moderately on SUSY parameters other than M_A and $\tan \beta$. In particular, they depend only weakly on possible new sources of flavor violation beyond the MFV ansatz.

The constraints from the FCNC decays on the $\tan \beta$ - M_A plane depend crucially on several parameters, in particular the Higgsino mass, μ , the stop trilinear coupling, A_t , the gluino mass, M_3 , the mass splitting of the left-handed squarks, ΔQ_{13} , and its alignment in flavor space, ζ . The current experimental bounds on the $\text{BR}(B_s \rightarrow \mu^+ \mu^-)$ lead to strong constraints in the large $\tan \beta$ regime of the MSSM with MFV. Constraints are particularly strong if the MSSM contributions interfere constructively with the SM, which happens for $\text{sign}(\mu A_t) = -1$. In that case, even for moderately large $\tan \beta \sim 30$, heavy Higgs masses of up to 1 TeV can be probed. Note that these bounds can have a strong dependence on ΔQ_{13} and ζ . For negative A_t , they become less constraining for larger values of ζ and larger ΔQ_{13} . The main dependence is to a good approximation on the product $\zeta \times \Delta Q_{13}$. In a mSUGRA setup this product is correlated with the mass splitting of the right-handed up squarks $\zeta \times \Delta Q_{13} \simeq \Delta U_{13}/2$. From our RGE analysis of a simple mSUGRA model, we expect $\zeta = 0.8$ for $\tan \beta = 45$ and ζ even closer to 1 for smaller $\tan \beta$. We also find $\Delta Q_{13} \sim 20\%$ to 35% , which should be approximately generic for SUSY breaking models with flavor universal soft masses at the GUT scale and light gluinos $M_3 \lesssim 2$ TeV. Such values have visible impact on the bounds derived from $\text{BR}(B_s \rightarrow \mu^+ \mu^-)$. If a lower bound on $\text{BR}(B_s \rightarrow \mu^+ \mu^-)$ above one half of the SM prediction is established in the future, destructively interfering SUSY contributions will also be highly constrained.

It is important to stress that the MSSM contributions to $B_s \rightarrow \mu^+ \mu^-$ do not necessarily decouple with the SUSY scale, but can probe masses of SUSY particles far above the scales that are currently reached by direct searches. On the other hand, the MSSM contributions to the $B \rightarrow X_s \gamma$ decay do decouple with the SUSY scale, but even so, the $B \rightarrow X_s \gamma$ decay can give non-trivial constraints on the MFV MSSM parameter space. If SUSY particles are heavier than ~ 2 TeV, charged Higgs contributions to $\text{BR}(B \rightarrow X_s \gamma)$ still lead to a constraint for small M_A which is almost independent of all other parameters if $\tan \beta$ is not large. The corresponding bound in the M_A - $\tan \beta$ plane can be stronger than the bounds from direct searches for $\tan \beta \lesssim 5$ and rules out $M_A \lesssim 300$ GeV if squarks are decoupled. For a TeV scale SUSY spectrum, SUSY loops can also contribute sizably to $B \rightarrow X_s \gamma$. This is particularly true for a sizable mass splitting ΔQ_{13} and negative values of

A_t , where Higgsino and gluino loop contributions add up constructively. Again, ζ can impact the implied constraints significantly. In contrast to $B_s \rightarrow \mu^+ \mu^-$, however, the bounds become stronger for larger values of ζ , if A_t is negative. A main conclusion of our work is that the current bounds from $B \rightarrow X_s \gamma$ and $B_s \rightarrow \mu^+ \mu^-$ are minimized if both μ and A_t are positive. In this region of parameter space, $(g-2)_\mu$ generically prefers a positive sign of M_2 .

We remark that the discussed FCNC B decays are also sensitive to sources of flavor violation beyond MFV. For the MSSM with generic flavor violating structures, however, bounds from FCNC processes become significantly more model dependent.

Finally, we analyzed the impact of the updated bounds from dark matter direct detection searches. We found that the parameter space region where $M_1 \simeq \mu$ is ruled out throughout the whole M_A - $\tan \beta$ plane. Away from bino-higgsino degeneracy, the current Xenon100 bounds still give strong constraints in the M_A - $\tan \beta$ plane as long as M_1 and μ are below 1 TeV and μ is positive. The direct detection bounds are minimized for negative μ , where light and heavy scalar contributions to the neutralino-proton cross section partially cancel. These direct detection constraints are the least robust among the considered bounds, since they are subject to important nuclear and astrophysical uncertainties and depend crucially on the assumption that the lightest MSSM neutralino constitutes the entire dark matter in the universe.

In summary, we presented the viable MSSM parameter space using the MFV assumption, incorporating the discovery of a Higgs state at 125 GeV, the null direct search results for supersymmetric particles and for $H/A \rightarrow \tau^+ \tau^-$ and bb , and constraints from B and K observables as well as dark matter direct detection searches. We also discussed and imposed electroweak vacuum meta-stability requirements, and we illustrated expectations for B flavor bounds arising from a renormalization group running analysis of generic minimal supergravity models. Throughout, we have emphasized the connection between flavor observables and direct collider searches in exploring the MSSM parameter space. This complementarity is not only important for understanding the present status of the MSSM with MFV, but it is also central to interpreting future experimental discoveries.

ACKNOWLEDGMENTS

We would like to acknowledge helpful discussions with Stefania Gori, Arjun Menon and Carlos Wagner. We thank the Aspen Center for Physics for warm hospitality where part of this work was completed. The Aspen Center for Physics is supported by the National Science Foundation Grant No. PHY-1066293. W.A. thanks the Galileo Galilei Institute for Theoretical Physics for warm hospitality and the INFN for partial support during the completion of this work. Fermilab is operated by Fermi

Research Alliance, LLC under Contract No. De-AC02-07CH11359 with the United States Department of Energy. N.R.S is supported by the DoE grant No. DE-SC0007859.

APPENDIX: LOOP FUNCTIONS

The loop induced “wrong” Higgs couplings involve a single loop function

$$g(x, y, z) = \frac{x \log x}{(x-y)(x-z)} + \frac{y \log y}{(y-x)(y-z)} + \frac{z \log z}{(z-x)(z-y)} .$$

The loop functions $h_{7,8}$ enter the charged Higgs contributions to the $b \rightarrow s\gamma$ transition

$$h_7(x) = \frac{3-5x}{12(1-x)^2} + \frac{2-3x}{6(1-x)^3} \log x ,$$

$$h_8(x) = \frac{3-x}{4(1-x)^2} + \frac{1}{2(1-x)^3} \log x .$$

The loop functions that enter the Higgsino, gluino, and Wino contributions to the $b \rightarrow s\gamma$ transition can be writ-

ten as

$$f_7^{\hat{H}} = f_1 + \frac{2}{3}f_2 , \quad f_7^{\hat{g}} = -\frac{8}{9}f_2 , \quad f_7^{\hat{W}} = -f_3 - \frac{1}{2}f_2 ,$$

$$f_8^{\hat{H}} = f_2 , \quad f_8^{\hat{g}} = -\frac{1}{3}f_2 - 3f_1 , \quad f_8^{\hat{W}} = -\frac{3}{2}f_2 ,$$

with

$$f_1(x, y, z) = -\frac{x^2 \log x}{(x-y)(x-z)^3} - \frac{y^2 \log y}{(y-x)(y-z)^3} - \frac{(x^2 y^2 - 3xyz^2 + (x+y)z^3) \log z}{(x-z)^3(y-z)^3} + \frac{x(z-3y) + z(y+z)}{2(x-z)^2(y-z)^2} ,$$

$$f_2(x, y, z) = \frac{xz \log x}{(x-y)(x-z)^3} + \frac{yz \log y}{(y-x)(y-z)^3} + \frac{z(xy(x+y) - 3xyz + z^3) \log z}{(x-z)^3(y-z)^3} + \frac{z(y-3z) + x(y+z)}{2(x-z)^2(y-z)^2} ,$$

$$f_3(x, y, z) = -\frac{z^2 \log x}{(x-y)(x-z)^3} - \frac{z^2 \log y}{(y-x)(y-z)^3} - \frac{z^2(x^2 + xy + y^2 - 3(x+y)z + 3z^2) \log z}{(x-z)^3(y-z)^3} + \frac{x(y-3z) + z(5z-3y)}{2(x-z)^2(y-z)^2} .$$

-
- | | |
|--|---|
| <p>[1] G. Aad <i>et al.</i> [ATLAS Collaboration], arXiv:1210.4826 [hep-ex].</p> <p>[2] G. Aad <i>et al.</i> [ATLAS Collaboration], arXiv:1210.4813 [hep-ex].</p> <p>[3] G. Aad <i>et al.</i> [ATLAS Collaboration], arXiv:1210.4457 [hep-ex].</p> <p>[4] G. Aad <i>et al.</i> [ATLAS Collaboration], arXiv:1210.4491 [hep-ex].</p> <p>[5] G. Aad <i>et al.</i> [ATLAS Collaboration], arXiv:1210.2852 [hep-ex].</p> <p>[6] G. Aad <i>et al.</i> [ATLAS Collaboration], arXiv:1210.1314 [hep-ex].</p> <p>[7] G. Aad <i>et al.</i> [ATLAS Collaboration], arXiv:1209.4625 [hep-ex].</p> <p>[8] G. Aad <i>et al.</i> [ATLAS Collaboration], arXiv:1209.4186 [hep-ex].</p> <p>[9] G. Aad <i>et al.</i> [ATLAS Collaboration], arXiv:1209.2102 [hep-ex].</p> <p>[10] G. Aad <i>et al.</i> [ATLAS Collaboration], arXiv:1209.0753 [hep-ex].</p> <p>[11] G. Aad <i>et al.</i> [ATLAS Collaboration], arXiv:1208.4688 [hep-ex].</p> <p>[12] G. Aad <i>et al.</i> [ATLAS Collaboration], arXiv:1208.4305 [hep-ex].</p> <p>[13] G. Aad <i>et al.</i> [ATLAS Collaboration], arXiv:1208.3144 [hep-ex].</p> | <p>[14] G. Aad <i>et al.</i> [ATLAS Collaboration], arXiv:1208.2884 [hep-ex].</p> <p>[15] G. Aad <i>et al.</i> [ATLAS Collaboration], arXiv:1208.2590 [hep-ex].</p> <p>[16] G. Aad <i>et al.</i> [ATLAS Collaboration], arXiv:1208.1447 [hep-ex].</p> <p>[17] G. Aad <i>et al.</i> [ATLAS Collaboration], arXiv:1208.0949 [hep-ex].</p> <p>[18] G. Aad <i>et al.</i> [ATLAS Collaboration], arXiv:1207.4686 [hep-ex].</p> <p>[19] G. Aad <i>et al.</i> [ATLAS Collaboration], JHEP 1207, 167 (2012) [arXiv:1206.1760 [hep-ex]].</p> <p>[20] S. Chatrchyan <i>et al.</i> [CMS Collaboration], Phys. Lett. B 716, 260 (2012) [arXiv:1204.3774 [hep-ex]].</p> <p>[21] S. Chatrchyan <i>et al.</i> [CMS Collaboration], JHEP 1206, 169 (2012) [arXiv:1204.5341 [hep-ex]].</p> <p>[22] S. Chatrchyan <i>et al.</i> [CMS Collaboration], JHEP 1208, 110 (2012) [arXiv:1205.3933 [hep-ex]].</p> <p>[23] S. Chatrchyan <i>et al.</i> [CMS Collaboration], Phys. Rev. Lett. 109, 071803 (2012) [arXiv:1205.6615 [hep-ex]].</p> <p>[24] S. Chatrchyan <i>et al.</i> [CMS Collaboration], arXiv:1206.3949 [hep-ex].</p> <p>[25] S. Chatrchyan <i>et al.</i> [CMS Collaboration], arXiv:1207.1898 [hep-ex].</p> <p>[26] S. Chatrchyan <i>et al.</i> [CMS Collaboration], arXiv:1207.1798 [hep-ex].</p> |
|--|---|

- [27] S. Chatrchyan *et al.* [CMS Collaboration], arXiv:1208.4859 [hep-ex].
- [28] S. Chatrchyan *et al.* [CMS Collaboration], arXiv:1209.6620 [hep-ex].
- [29] S. Chatrchyan *et al.* [CMS Collaboration], arXiv:1210.2052 [hep-ex].
- [30] G. Aad *et al.* [ATLAS Collaboration], Phys. Lett. B **716**, 1 (2012) [arXiv:1207.7214 [hep-ex]].
- [31] S. Chatrchyan *et al.* [CMS Collaboration], Phys. Lett. B **716**, 30 (2012) [arXiv:1207.7235 [hep-ex]].
- [32] L. J. Hall, D. Pinner and J. T. Ruderman, JHEP **1204**, 131 (2012) [arXiv:1112.2703 [hep-ph]].
- [33] H. Baer, V. Barger and A. Mustafayev, Phys. Rev. D **85**, 075010 (2012) [arXiv:1112.3017 [hep-ph]].
- [34] J. L. Feng, K. T. Matchev and D. Sanford, Phys. Rev. D **85**, 075007 (2012) [arXiv:1112.3021 [hep-ph]].
- [35] S. Heinemeyer, O. Stal and G. Weiglein, Phys. Lett. B **710**, 201 (2012) [arXiv:1112.3026 [hep-ph]].
- [36] A. Arbey, M. Battaglia, A. Djouadi, F. Mahmoudi and J. Quevillon, Phys. Lett. B **708**, 162 (2012) [arXiv:1112.3028 [hep-ph]].
- [37] A. Arbey, M. Battaglia and F. Mahmoudi, Eur. Phys. J. C **72**, 1906 (2012) [arXiv:1112.3032 [hep-ph]].
- [38] P. Draper, P. Meade, M. Reece and D. Shih, Phys. Rev. D **85**, 095007 (2012) [arXiv:1112.3068 [hep-ph]].
- [39] M. Carena, S. Gori, N. R. Shah and C. E. M. Wagner, JHEP **1203**, 014 (2012) [arXiv:1112.3336 [hep-ph]].
- [40] U. Ellwanger, JHEP **1203**, 044 (2012) [arXiv:1112.3548 [hep-ph]].
- [41] O. Buchmueller, R. Cavanaugh, A. De Roeck, M. J. Dolan, J. R. Ellis, H. Flacher, S. Heinemeyer and G. Isidori *et al.*, Eur. Phys. J. C **72**, 2020 (2012) [arXiv:1112.3564 [hep-ph]].
- [42] S. Akula, B. Altunkaynak, D. Feldman, P. Nath and G. Peim, Phys. Rev. D **85**, 075001 (2012) [arXiv:1112.3645 [hep-ph]].
- [43] M. Kadastik, K. Kannike, A. Racioppi and M. Raidal, JHEP **1205**, 061 (2012) [arXiv:1112.3647 [hep-ph]].
- [44] J. Cao, Z. Heng, D. Li and J. M. Yang, Phys. Lett. B **710**, 665 (2012) [arXiv:1112.4391 [hep-ph]].
- [45] J. F. Guinon, Y. Jiang and S. Kraml, Phys. Lett. B **710**, 454 (2012) [arXiv:1201.0982 [hep-ph]].
- [46] S. F. King, M. Muhlleitner and R. Nevzorov, Nucl. Phys. B **860**, 207 (2012) [arXiv:1201.2671 [hep-ph]].
- [47] Z. Kang, J. Li and T. Li, JHEP **1211**, 024 (2012) [arXiv:1201.5305 [hep-ph]].
- [48] L. Aparicio, D. G. Cerdeno and L. E. Ibanez, JHEP **1204**, 126 (2012) [arXiv:1202.0822 [hep-ph]].
- [49] J. Ellis, K. A. Olive and K. A. Olive, Eur. Phys. J. C **72**, 2005 (2012) [arXiv:1202.3262 [hep-ph]].
- [50] H. Baer, V. Barger and A. Mustafayev, JHEP **1205**, 091 (2012) [arXiv:1202.4038 [hep-ph]].
- [51] J. -J. Cao, Z. -X. Heng, J. M. Yang, Y. -M. Zhang and J. -Y. Zhu, JHEP **1203**, 086 (2012) [arXiv:1202.5821 [hep-ph]].
- [52] L. Maiani, A. D. Polosa and V. Riquer, New J. Phys. **14**, 073029 (2012) [arXiv:1202.5998 [hep-ph]].
- [53] N. D. Christensen, T. Han and S. Su, Phys. Rev. D **85**, 115018 (2012) [arXiv:1203.3207 [hep-ph]].
- [54] D. A. Vasquez, G. Belanger, C. Boehm, J. Da Silva, P. Richardson and C. Wymant, Phys. Rev. D **86**, 035023 (2012) [arXiv:1203.3446 [hep-ph]].
- [55] M. A. Ajaib, I. Gogoladze, F. Nasir and Q. Shafi, Phys. Lett. B **713**, 462 (2012) [arXiv:1204.2856 [hep-ph]].
- [56] F. Brummer, S. Kraml and S. Kulkarni, JHEP **1208**, 089 (2012) [arXiv:1204.5977 [hep-ph]].
- [57] J. L. Feng and D. Sanford, Phys. Rev. D **86**, 055015 (2012) [arXiv:1205.2372 [hep-ph]].
- [58] M. Carena, S. Gori, N. R. Shah, C. E. M. Wagner and L. -T. Wang, JHEP **1207**, 175 (2012) [arXiv:1205.5842 [hep-ph]].
- [59] A. Fowlie, M. Kazana, K. Kowalska, S. Munir, L. Roszkowski, E. M. Sessolo, S. Trojanowski and Y. -L. S. Tsai, arXiv:1206.0264 [hep-ph].
- [60] K. Blum, R. T. D'Agnolo and J. Fan, arXiv:1206.5303 [hep-ph].
- [61] M. W. Cahill-Rowley, J. L. Hewett, A. Ismail and T. G. Rizzo, arXiv:1206.5800 [hep-ph].
- [62] R. Benbrik, M. G. Bock, S. Heinemeyer, O. Stal, G. Weiglein and L. Zeune, arXiv:1207.1096 [hep-ph].
- [63] A. Arbey, M. Battaglia, A. Djouadi and F. Mahmoudi, JHEP **1209**, 107 (2012) [arXiv:1207.1348 [hep-ph]].
- [64] S. Akula, P. Nath and G. Peim, Phys. Lett. B **717**, 188 (2012) [arXiv:1207.1839 [hep-ph]].
- [65] H. An, T. Liu and L. -T. Wang, arXiv:1207.2473 [hep-ph].
- [66] J. Cao, Z. Heng, J. M. Yang and J. Zhu, JHEP **1210**, 079 (2012) [arXiv:1207.3698 [hep-ph]].
- [67] G. F. Giudice, P. Paradisi and A. Strumia, arXiv:1207.6393 [hep-ph].
- [68] O. Buchmueller, R. Cavanaugh, M. Citron, A. De Roeck, M. J. Dolan, J. R. Ellis, H. Flacher and S. Heinemeyer *et al.*, arXiv:1207.7315 [hep-ph].
- [69] J. R. Espinosa, C. Grojean, V. Sanz and M. Trott, arXiv:1207.7355 [hep-ph].
- [70] K. Schmidt-Hoberg and F. Staub, arXiv:1208.1683 [hep-ph].
- [71] F. Boudjema and G. D. La Rochelle, arXiv:1208.1952 [hep-ph].
- [72] L. Maiani, A. D. Polosa and V. Riquer, arXiv:1209.4816 [hep-ph].
- [73] H. Baer, V. Barger, P. Huang, D. Mickelson, A. Mustafayev and X. Tata, arXiv:1210.3019 [hep-ph].
- [74] M. Drees, arXiv:1210.6507 [hep-ph].
- [75] U. Haisch and F. Mahmoudi, arXiv:1210.7806 [hep-ph].
- [76] CDF and D0 Collaborations, arXiv:1207.0449 [hep-ex].
- [77] CMS Collaboration, CMS-PAS-HIG-12-050.
- [78] CMS Collaboration, CMS-PAS-HIG-12-026.
- [79] CMS Collaboration, CMS-PAS-HIG-12-027.
- [80] R. Aaij *et al.* [LHCb Collaboration], arXiv:1211.2674 [hep-ex].
- [81] I. Adachi *et al.* [Belle Collaboration], arXiv:1208.4678 [hep-ex].
- [82] BaBar Collaboration, arXiv:1207.0698 [hep-ex].
- [83] J. P. Lees *et al.* [BABAR Collaboration], arXiv:1207.5772 [hep-ex].
- [84] XENON100 Collaboration, arXiv:1207.5988 [astro-ph.CO].
- [85] G. D'Ambrosio, G. F. Giudice, G. Isidori and A. Strumia, Nucl. Phys. B **645**, 155 (2002) [hep-ph/0207036].
- [86] R. S. Chivukula and H. Georgi, Phys. Lett. B **188**, 99 (1987).
- [87] L. J. Hall and L. Randall, Phys. Rev. Lett. **65**, 2939 (1990).
- [88] A. J. Buras, P. Gambino, M. Gorbahn, S. Jager and L. Silvestrini, Phys. Lett. B **500**, 161 (2001) [hep-ph/0007085].
- [89] M. S. Carena, A. Menon, R. Noriega-Papaqui,

- A. Szykman and C. E. M. Wagner, Phys. Rev. D **74**, 015009 (2006) [hep-ph/0603106].
- [90] M. S. Carena, A. Menon and C. E. M. Wagner, Phys. Rev. D **76**, 035004 (2007) [arXiv:0704.1143 [hep-ph]].
- [91] M. Carena, A. Menon and C. E. M. Wagner, Phys. Rev. D **79**, 075025 (2009) [arXiv:0812.3594 [hep-ph]].
- [92] P. Paradisi, M. Ratz, R. Schieren and C. Simonetto, Phys. Lett. B **668**, 202 (2008) [arXiv:0805.3989 [hep-ph]].
- [93] G. Colangelo, E. Nikolidakis and C. Smith, Eur. Phys. J. C **59**, 75 (2009) [arXiv:0807.0801 [hep-ph]].
- [94] C. F. Berger, J. S. Gainer, J. L. Hewett and T. G. Rizzo, JHEP **0902**, 023 (2009) [arXiv:0812.0980 [hep-ph]].
- [95] A. Crivellin, Phys. Rev. D **83**, 056001 (2011) [arXiv:1012.4840 [hep-ph]].
- [96] A. Crivellin, L. Hofer and J. Rosiek, JHEP **1107**, 017 (2011) [arXiv:1103.4272 [hep-ph]].
- [97] M. S. Carena, M. Quiros and C. E. M. Wagner, Nucl. Phys. B **461**, 407 (1996) [hep-ph/9508343].
- [98] R. Hempfling, Phys. Rev. D **49**, 6168 (1994).
- [99] L. J. Hall, R. Rattazzi and U. Sarid, Phys. Rev. D **50**, 7048 (1994) [hep-ph/9306309].
- [100] M. S. Carena, M. Olechowski, S. Pokorski and C. E. M. Wagner, Nucl. Phys. B **426**, 269 (1994) [hep-ph/9402253].
- [101] B. A. Dobrescu and P. J. Fox, Eur. Phys. J. C **70**, 263 (2010) [arXiv:1001.3147 [hep-ph]].
- [102] T. Blazek, S. Raby and S. Pokorski, Phys. Rev. D **52**, 4151 (1995) [hep-ph/9504364].
- [103] M. S. Carena, D. Garcia, U. Nierste and C. E. M. Wagner, Nucl. Phys. B **577**, 88 (2000) [hep-ph/9912516].
- [104] M. S. Carena, D. Garcia, U. Nierste and C. E. M. Wagner, Phys. Lett. B **499**, 141 (2001) [hep-ph/0010003].
- [105] C. Hamzaoui, M. Pospelov and M. Toharia, Phys. Rev. D **59**, 095005 (1999) [hep-ph/9807350].
- [106] K. S. Babu and C. F. Kolda, Phys. Rev. Lett. **84**, 228 (2000) [hep-ph/9909476].
- [107] G. Isidori and A. Retico, JHEP **0111**, 001 (2001) [hep-ph/0110121].
- [108] A. Dedes and A. Pilaftsis, Phys. Rev. D **67**, 015012 (2003) [hep-ph/0209306].
- [109] A. J. Buras, P. H. Chankowski, J. Rosiek and L. Slawianowska, Nucl. Phys. B **659**, 3 (2003) [hep-ph/0210145].
- [110] L. Hofer, U. Nierste and D. Scherer, JHEP **0910**, 081 (2009) [arXiv:0907.5408 [hep-ph]].
- [111] T. Aaltonen *et al.* [CDF Collaboration], Phys. Rev. Lett. **103**, 201801 (2009) [arXiv:0906.1014 [hep-ex]].
- [112] V. M. Abazov *et al.* [D0 Collaboration], Phys. Lett. B **707**, 323 (2012) [arXiv:1106.4555 [hep-ex]].
- [113] V. M. Abazov *et al.* [D0 Collaboration], Phys. Rev. Lett. **107**, 121801 (2011) [arXiv:1106.4885 [hep-ex]].
- [114] T. Aaltonen *et al.* [CDF and D0 Collaborations], arXiv:1207.2757 [hep-ex].
- [115] S. Chatrchyan *et al.* [CMS Collaboration], Phys. Lett. B **713**, 68 (2012) [arXiv:1202.4083 [hep-ex]].
- [116] Atlas Collaboration, ATLAS-CONF-2012-094.
- [117] V. M. Abazov *et al.* [D0 Collaboration], Phys. Lett. B **682**, 278 (2009) [arXiv:0908.1811 [hep-ex]].
- [118] T. Aaltonen *et al.* [CDF Collaboration], Phys. Rev. Lett. **103**, 101803 (2009) [arXiv:0907.1269 [hep-ex]].
- [119] G. Aad *et al.* [ATLAS Collaboration], JHEP **1206**, 039 (2012) [arXiv:1204.2760 [hep-ex]].
- [120] ATLAS Collaboration, ATLAS-CONF-2011-094
- [121] S. Chatrchyan *et al.* [CMS Collaboration], JHEP **1207**, 143 (2012) [arXiv:1205.5736 [hep-ex]].
- [122] M. Spira, hep-ph/9510347.
- [123] R. V. Harlander and W. B. Kilgore, Phys. Rev. D **68**, 013001 (2003) [hep-ph/0304035].
- [124] A. Djouadi, J. Kalinowski and M. Spira, Comput. Phys. Commun. **108**, 56 (1998) [hep-ph/9704448].
- [125] S. Heinemeyer, W. Hollik and G. Weiglein, Comput. Phys. Commun. **124**, 76 (2000) [hep-ph/9812320].
- [126] M. S. Carena, S. Heinemeyer, C. E. M. Wagner and G. Weiglein, Eur. Phys. J. C **26**, 601 (2003) [hep-ph/0202167].
- [127] M. S. Carena, S. Heinemeyer, C. E. M. Wagner and G. Weiglein, Eur. Phys. J. C **45**, 797 (2006) [hep-ph/0511023].
- [128] M. Carena, S. Gori, A. Juste, A. Menon, C. E. M. Wagner and L. -T. Wang, JHEP **1207**, 091 (2012) [arXiv:1203.1041 [hep-ph]].
- [129] J. Hisano and S. Sugiyama, Phys. Lett. B **696**, 92 (2011) [arXiv:1011.0260 [hep-ph]]. Claudson:1983et,Kusenko:1996jn
- [130] M. Claudson, L. J. Hall and I. Hinchliffe, Nucl. Phys. B **228**, 501 (1983).
- [131] A. Kusenko, P. Langacker and G. Segre, Phys. Rev. D **54**, 5824 (1996) [hep-ph/9602414].
- [132] M. J. Duncan and L. G. Jensen, Phys. Lett. B **291**, 109 (1992).
- [133] C. L. Wainwright, Comput. Phys. Commun. **183**, 2006 (2012) [arXiv:1109.4189 [hep-ph]].
- [134] S. Bertolini, F. Borzumati, A. Masiero and G. Ridolfi, Nucl. Phys. B **353**, 591 (1991).
- [135] T. Goto, Y. Okada and Y. Shimizu, Phys. Rev. D **58**, 094006 (1998) [hep-ph/9804294].
- [136] G. Isidori and P. Paradisi, Phys. Lett. B **639**, 499 (2006) [hep-ph/0605012].
- [137] W. Altmannshofer, A. J. Buras and D. Guadagnoli, JHEP **0711**, 065 (2007) [hep-ph/0703200].
- [138] F. Domingo and U. Ellwanger, JHEP **0712**, 090 (2007) [arXiv:0710.3714 [hep-ph]].
- [139] M. Wick and W. Altmannshofer, AIP Conf. Proc. **1078**, 348 (2009) [arXiv:0810.2874 [hep-ph]].
- [140] W. Altmannshofer and D. M. Straub, JHEP **1009**, 078 (2010) [arXiv:1004.1993 [hep-ph]].
- [141] F. Gabbiani, E. Gabrielli, A. Masiero and L. Silvestrini, Nucl. Phys. B **477**, 321 (1996) [hep-ph/9604387].
- [142] S. Baek, T. Goto, Y. Okada and K. -i. Okumura, Phys. Rev. D **64**, 095001 (2001) [hep-ph/0104146].
- [143] J. Foster, K. -i. Okumura and L. Roszkowski, JHEP **0508**, 094 (2005) [hep-ph/0506146].
- [144] G. F. Giudice, M. Nardecchia and A. Romanino, Nucl. Phys. B **813**, 156 (2009) [arXiv:0812.3610 [hep-ph]].
- [145] W. Altmannshofer, A. J. Buras, S. Gori, P. Paradisi and D. M. Straub, Nucl. Phys. B **830**, 17 (2010) [arXiv:0909.1333 [hep-ph]].
- [146] A. Crivellin and M. Davidkov, Phys. Rev. D **81**, 095004 (2010) [arXiv:1002.2653 [hep-ph]].
- [147] R. Barbieri, G. Isidori, J. Jones-Perez, P. Lodone and D. M. Straub, Eur. Phys. J. C **71**, 1725 (2011) [arXiv:1105.2296 [hep-ph]].
- [148] A. Crivellin, L. Hofer, U. Nierste and D. Scherer, Phys. Rev. D **84**, 035030 (2011) [arXiv:1105.2818 [hep-ph]].
- [149] L. Calibbi, R. N. Hodgkinson, J. Jones Perez, A. Masiero and O. Vives, Eur. Phys. J. C **72**, 1863 (2012) [arXiv:1111.0176 [hep-ph]].

- [150] G. Elor, L. J. Hall, D. Pinner and J. T. Ruderman, *JHEP* **1210**, 111 (2012) [arXiv:1206.5301 [hep-ph]].
- [151] W. -S. Hou, *Phys. Rev. D* **48**, 2342 (1993).
- [152] K. Nakamura *et al.* [Particle Data Group Collaboration], *J. Phys. G* **37**, 075021 (2010).
- [153] C. McNeile *et al.*, *Phys. Rev. D* **85**, 031503 (2012) [arXiv:1110.4510 [hep-lat]].
- [154] A. Bazavov *et al.* [Fermilab Lattice and MILC Collaboration], *Phys. Rev. D* **85**, 114506 (2012) [arXiv:1112.3051 [hep-lat]].
- [155] H. Na, C. J. Monahan, C. T. H. Davies, R. Horgan, G. P. Lepage and J. Shigemitsu, *Phys. Rev. D* **86**, 034506 (2012) [arXiv:1202.4914 [hep-lat]].
- [156] C. Davies, *PoS LATTICE 2011*, 019 (2011) [arXiv:1203.3862 [hep-lat]].
- [157] B. Aubert *et al.* [BaBar Collaboration], *Phys. Rev. D* **81**, 051101 (2010) [arXiv:0809.4027 [hep-ex]].
- [158] K. Hara *et al.* [Belle collaboration], *Phys. Rev. D* **82**, 071101 (2010) [arXiv:1006.4201 [hep-ex]].
- [159] M. Tanaka, *Z. Phys. C* **67**, 321 (1995) [hep-ph/9411405].
- [160] U. Nierste, S. Trine and S. Westhoff, *Phys. Rev. D* **78**, 015006 (2008) [arXiv:0801.4938 [hep-ph]].
- [161] J. F. Kamenik and F. Mescia, *Phys. Rev. D* **78**, 014003 (2008) [arXiv:0802.3790 [hep-ph]].
- [162] S. Fajfer, J. F. Kamenik and I. Nisandzic, *Phys. Rev. D* **85**, 094025 (2012) [arXiv:1203.2654 [hep-ph]].
- [163] D. Becirevic, N. Kosnik and A. Tayduganov, *Phys. Lett. B* **716**, 208 (2012) [arXiv:1206.4977 [hep-ph]].
- [164] J. A. Bailey, A. Bazavov, C. Bernard, C. M. Bouchard, C. DeTar, D. Du, A. X. El-Khadra and J. Foley *et al.*, *Phys. Rev. Lett.* **109**, 071802 (2012) [arXiv:1206.4992 [hep-ph]].
- [165] J. P. Lees *et al.* [BaBar Collaboration], *Phys. Rev. Lett.* **109**, 101802 (2012) [arXiv:1205.5442 [hep-ex]].
- [166] A. Bozek *et al.* [Belle Collaboration], *Phys. Rev. D* **82**, 072005 (2010) [arXiv:1005.2302 [hep-ex]].
- [167] M. Antonelli, V. Cirigliano, G. Isidori, F. Mescia, M. Moulson, H. Neufeld, E. Passemar and M. Palutan *et al.*, *Eur. Phys. J. C* **69**, 399 (2010) [arXiv:1005.2323 [hep-ph]].
- [168] S. Fajfer, J. F. Kamenik, I. Nisandzic and J. Zupan, arXiv:1206.1872 [hep-ph].
- [169] A. Crivellin, C. Greub and A. Kokulu, *Phys. Rev. D* **86**, 054014 (2012) [arXiv:1206.2634 [hep-ph]].
- [170] A. Datta, M. Duraisamy and D. Ghosh, *Phys. Rev. D* **86**, 034027 (2012) [arXiv:1206.3760 [hep-ph]].
- [171] N. G. Deshpande and A. Menon, arXiv:1208.4134 [hep-ph].
- [172] A. Celis, M. Jung, X. -Q. Li and A. Pich, arXiv:1210.8443 [hep-ph].
- [173] K. De Bruyn, R. Fleischer, R. Knegjens, P. Koppenburg, M. Merk and N. Tuning, *Phys. Rev. D* **86**, 014027 (2012) [arXiv:1204.1735 [hep-ph]].
- [174] K. De Bruyn, R. Fleischer, R. Knegjens, P. Koppenburg, M. Merk, A. Pellegrino and N. Tuning, *Phys. Rev. Lett.* **109**, 041801 (2012) [arXiv:1204.1737 [hep-ph]].
- [175] W. Altmannshofer and D. M. Straub, *JHEP* **1208**, 121 (2012) [arXiv:1206.0273 [hep-ph]].
- [176] A. J. Buras, J. Girrbach, D. Guadagnoli and G. Isidori, arXiv:1208.0934 [hep-ph].
- [177] V. M. Abazov *et al.* [D0 Collaboration], *Phys. Lett. B* **693**, 539 (2010) [arXiv:1006.3469 [hep-ex]].
- [178] T. Aaltonen *et al.* [CDF Collaboration], *Phys. Rev. Lett.* **107**, 239903 (2011) [Phys. Rev. Lett. **107**, 191801 (2011)] [arXiv:1107.2304 [hep-ex]], update with the full CDF dataset at www-cdf.fnal.gov/physics/new/bottom/bottom.html.
- [179] G. Aad *et al.* [ATLAS Collaboration], *Phys. Lett. B* **713**, 387 (2012) [arXiv:1204.0735 [hep-ex]].
- [180] S. Chatrchyan *et al.* [CMS Collaboration], *JHEP* **1204**, 033 (2012) [arXiv:1203.3976 [hep-ex]].
- [181] R. Aaij *et al.* [LHCb Collaboration], *Phys. Rev. Lett.* **108**, 231801 (2012) [arXiv:1203.4493 [hep-ex]].
- [182] LHCb, CMS, and ATLAS Collaborations, LHCb-CONF-2012-017, CMS-PAS-BPH-12-009, ATLAS-CONF-2012-061.
- [183] S. R. Choudhury and N. Gaur, *Phys. Lett. B* **451**, 86 (1999) [hep-ph/9810307].
- [184] J. Abdallah *et al.* [DELPHI Collaboration], *Eur. Phys. J. C* **31**, 421 (2003) [hep-ex/0311019].
- [185] G. Abbiendi *et al.* [OPAL Collaboration], *Eur. Phys. J. C* **35**, 1 (2004) [hep-ex/0401026].
- [186] I. Bediaga *et al.* [LHCb Collaboration], CERN-LHCC-2012-007, LHCb-TDR-012.
- [187] H. E. Logan and U. Nierste, *Nucl. Phys. B* **586**, 39 (2000) [hep-ph/0004139].
- [188] M. Misiak *et al.*, *Phys. Rev. Lett.* **98**, 022002 (2007) [hep-ph/0609232].
- [189] T. Becher and M. Neubert, *Phys. Rev. Lett.* **98**, 022003 (2007) [hep-ph/0610067].
- [190] M. Benzke, S. J. Lee, M. Neubert and G. Paz, *JHEP* **1008**, 099 (2010) [arXiv:1003.5012 [hep-ph]].
- [191] Y. Amhis *et al.* [HFAG Collaboration], arXiv:1207.1158 [hep-ex], and online update at <http://www.slac.stanford.edu/xorg/hfag/>.
- [192] A. Freitas and U. Haisch, *Phys. Rev. D* **77**, 093008 (2008) [arXiv:0801.4346 [hep-ph]].
- [193] W. Altmannshofer, P. Paradisi and D. M. Straub, *JHEP* **1204**, 008 (2012) [arXiv:1111.1257 [hep-ph]].
- [194] S. P. Martin and M. T. Vaughn, *Phys. Rev. D* **50**, 2282 (1994) [Erratum-ibid. *D* **78**, 039903 (2008)] [hep-ph/9311340].
- [195] D. M. Pierce, J. A. Bagger, K. T. Matchev and R. -j. Zhang, *Nucl. Phys. B* **491**, 3 (1997) [hep-ph/9606211].
- [196] L. E. Ibanez and C. Lopez, *Nucl. Phys. B* **233**, 511 (1984).
- [197] L. E. Ibanez, C. Lopez and C. Munoz, *Nucl. Phys. B* **256**, 218 (1985).
- [198] M. S. Carena, M. Olechowski, S. Pokorski and C. E. M. Wagner, *Nucl. Phys. B* **419**, 213 (1994) [hep-ph/9311222].
- [199] N. Arkani-Hamed, A. Delgado and G. F. Giudice, *Nucl. Phys. B* **741**, 108 (2006) [hep-ph/0601041].
- [200] G. B. Gelmini and P. Gondolo, *Phys. Rev. D* **74**, 023510 (2006) [hep-ph/0602230].
- [201] M. Srednicki and R. Watkins, *Phys. Lett. B* **225**, 140 (1989).
- [202] G. B. Gelmini, P. Gondolo and E. Roulet, *Nucl. Phys. B* **351**, 623 (1991).
- [203] M. Drees and M. Nojiri, *Phys. Rev. D* **48**, 3483 (1993) [hep-ph/9307208].
- [204] J. R. Ellis, A. Ferstl and K. A. Olive, *Phys. Lett. B* **481**, 304 (2000) [hep-ph/0001005].
- [205] J. R. Ellis, K. A. Olive, Y. Santoso and V. C. Spanos, *Phys. Rev. D* **71**, 095007 (2005) [hep-ph/0502001].
- [206] M. S. Carena, D. Hooper and P. Z. Skands, *Phys. Rev. Lett.* **97**, 051801 (2006) [hep-ph/0603180].
- [207] M. S. Carena, D. Hooper and A. Vallinotto, *Phys. Rev.*

- D **75**, 055010 (2007) [hep-ph/0611065].
- [208] C. Stenge, G. Bertone, D. G. Cerdeno, M. Fornasa, R. Ruiz de Austri and R. Trotta, JCAP **1203**, 030 (2012) [arXiv:1112.4192 [hep-ph]].
- [209] M. Perelstein and B. Shakya, arXiv:1208.0833 [hep-ph].
- [210] J. Giedt, A. W. Thomas and R. D. Young, Phys. Rev. Lett. **103**, 201802 (2009) [arXiv:0907.4177 [hep-ph]].
- [211] E. Aprile *et al.* [XENON100 Collaboration], Phys. Rev. Lett. **107**, 131302 (2011) [arXiv:1104.2549 [astro-ph.CO]].